MR-Visible Lipids and the Tumor Microenvironment

E. James Delikatny, **Sanjeev Chawla**, **Daniel-Joseph Leung**, and **Harish Poptani**
Department of Radiology, University of Pennsylvania School of Medicine, Philadelphia, PA 19104

Abstract

MR-visible lipids or mobile lipids are defined as lipids that are observable using proton magnetic resonance spectroscopy in cells and in tissues. These MR-visible lipids are composed of triglycerides and cholesterol esters that accumulate in intracellular neutral lipid droplets, where their MR visibility is conferred as a result of the increased molecular motion available in this unique physical environment. This review will discuss factors that lead to the biogenesis of MR-visible lipids in cancer cells and in other cell types such as immune cells and fibroblasts. We focus on the accumulations of mobile lipids that are inducible in cultured cells by a number of stresses, including culture conditions and in response to activating stimuli or apoptotic cell death induced by anticancer drugs. This is compared with animal tumor models, where increases in mobile lipids are observed in response to chemo and radiotherapy, and to human tumors where mobile lipids are observed predominantly in high-grade brain tumors and in regions of necrosis. Conducive conditions for mobile lipid formation in the tumor microenvironment will be discussed including low pH, oxygen availability and the presence of inflammatory cells. It is concluded that MR-visible lipids appear in cancer cells and human tumors as a stress response. Mobile lipids stored as neutral lipid droplets may play a role in detoxification of the cell or act as an alternate energy source, especially in cancer cells, which often grow in ischemic/hypoxic environments. The role of MR-visible lipids in cancer diagnosis and assessment of treatment response both in animal models of cancer as well as human brain tumors will also be discussed. Although technical limitations exist in the accurate detection of intratumoral mobile lipids, early increases in mobile lipids after therapeutic interventions may be used as a potential biomarker for assessing treatment response in cancer.

Keywords

Introduction

From the first irreparable mutation in carcinogenesis to the lodging and growth of the metastatic seed in foreign soil, the cancer cell faces hostile challenges affecting its survival, transport, and growth. The cancer cell must adapt to adjustments of the local tissue within the growing primary site, win the battle for essential nutrients and oxygen necessary to sustain growth, and survive the subsequent local acidosis, hypoxia, and starvation-induced autophagy of the tumor microenvironment. The successful metastatic cell employs increased mutagenic and metabolic adaptation to obtain the survival advantage over less well-adapted tumor and adjacent normal cells. It exploits the creation of new but imperfect vasculature to

---

[*]Correspondence to: E. James Delikatny, Ph.D., Molecular Imaging Laboratory, Department of Radiology, University of Pennsylvania School of Medicine, B6 Blockley Hall, 423 Guardian Drive, Philadelphia, PA 19104, Phone: (215) 898-3105; Fax: (215) 573-2113, delikatn@mail.med.upenn.edu.

feed the growing lesion, and negotiates the local accumulation of stromal cells and immune cells that accompany tumor growth. The invasive cells that survive must then navigate through the increasingly harsh hydrolytic environment needed to loosen the tight bounds of the extracellular matrix, and invade through the basement membrane only to find the lymphatic system or vasculature full of high-velocity flow, shear forces and aggressive immune cells. Lodging in the vasculature brings only a brief respite, for the cell must then find its way into a new tissue type, phenotypically readapt to the new environment and begin the seeding process again. This review article focuses on the metabolic adaptation of the cancer cell to the tumor microenvironment that can be detected non-invasively using *in vivo* proton magnetic resonance spectroscopy (MRS). The metabolites that contribute to the MR spectrum of cells and tumors will be explained, and both *in vitro* and *in vivo* studies will be used to demonstrate how conditions in the tumor microenvironment can alter MR-visible lipid metabolite levels. Although we will concentrate on changes in mobile lipid metabolites and the formation of triglycerides that often occur in response to stressful environments, we will discuss other metabolic changes as they relate to this phenomenon. The detection of mobile lipids and interpretation of their appearance in tumor models and in humans will also be discussed.

Proton MR spectra of cells and tissues

The proton MR spectra of cells and tissues contain three types of resonances, those arising from mobile side chains on peptides and proteins, those arising from mobile lipids and those arising from small molecular weight highly mobile metabolites that accumulate in millimolar or greater concentrations inside the cell [1](Table 1). Thus the ^{1}H MR spectrum of cells or tissues can be thought of as a superposition of the mobile protein and mobile lipid components observed in the cell, with additional contributions from the often cellular- or metabolically-specific small molecular weight metabolites. These metabolites include, but are not limited to, choline-containing metabolites (tCho), creatine (Cr) and phosphocreatine (PCr), lactate, *myo-* inositol, N-acetylaspartate (NAA, in the nervous system) and taurine.

Figure 1 shows ^{1}H MR spectra of human breast cancer cells before and after treatment with the antimitochondrial agent tetraphenylphosphonium chloride (TPP) [2]. The untreated cells (Fig 1A) display a spectrum predominantly consisting of the small molecular weight metabolites and of the mobile proteome, which we define as resonances from mobile amino acid side chains that may be free or in peptide form. The treated cells on the other hand show an increase in resonances arising from mobile lipids (Fig 1B). Potential regulatory factors governing this spectral transition will be discussed later in this article. At this juncture, the important point is the recognition that overlapping mobile amino acid and lipid resonances may make variable contributions to the observed ^{1}H MR spectrum.

In the majority of studies employing *in vivo* MR spectroscopy, resonances from the mobile proteome are not observed. This often results from the choice of a long echo time and a short repetition time that favor the observation of metabolites with longer T_2, the small molecular weight metabolites, since the concentration of these metabolites are often altered during disease progression or response to therapy. However, a number of recent studies have demonstrated the feasibility of short echo time MRS for the detection of mobile proteins [3-5]. These developments allow more detailed investigation of the mobile proteome, and its role in homeostasis and pathology.

In tumors, the most recognizable of the highly mobile metabolites is tCho, which resonates at 3.2 ppm and is a composite peak with contributions from choline, phosphocholine (PC), and glycerophosphocholine (GPC). An increase in the tCho resonance in tumors arises primarily from the synthesis and accumulation of PC, a metabolite produced by rapid uptake and phosphorylation of choline that is necessary for the downstream synthesis of

phosphatidylcholine, a major membrane phospholipid constituting around 25% of mammalian cellular lipids [6, 7]. The role of choline metabolites in the tumor microenvironment and in metastasis is reviewed elsewhere in this issue. As such, tCho and other small molecular weight metabolites will be discussed only when necessary to illustrate a specific point. This review focuses on the factors regulating the formation and maintenance of the mobile lipid phenotype, its role in the stress response with particular reference to the harsh conditions of the tumor microenvironment, and the advantages and potential pitfalls of observing these resonances in tumor cells, in animal tumor models and in human cancers.

Mobile or MR-Visible Lipids

MR-visible lipids, or as they are often called, mobile lipids, are lipids that are observable using high-resolution MRS or *in vivo* MR pulse sequences. The requirement for MR-visibility is that the lipid chains must possess sufficient rotational molecular freedom in order to motionally-narrow the MR lineshape. As such, MR-visible lipid resonances arise predominantly from triglycerides and cholesterol esters in neutral lipid droplets, and not from the lipids in membrane bilayers. The restricted molecular motion of bilayer lipid leads to dipolar broadening rendering them undetectable by standard MR techniques [8]. The role of MR-visible lipids in cancer and cancer diagnosis has been the subject of many excellent reviews and articles [9-12]. The present review focuses on controlling factors involved in stress-induced mobile lipids and how those factors may operate in the tumor microenvironment to influence observed MR spectra. Throughout this review the terms MR-visible lipids and mobile lipids are used interchangeably.

The MR-visible lipid spectrum consists of a number of resonances that are assigned in Table 1 and in Figure 1. The dominant resonances arise from protons on the fatty acyl chains, especially those arising from methylene ($-CH_2-CH_2-CH_2-$) and methyl (CH_3-CH_2-) groups at 1.3 and 0.9 ppm respectively. Other resonances arise from protons directly bonded to (-CH=CH-, 5.3 ppm) or one carbon removed from unsaturated carbons (the bis allylic -CH=CH-CH_2-CH=CH- at 2.8 ppm and the mono allylic -CH=CH-CH_2- at 2.0 ppm) in mono and polyunsaturated lipids. An additional group of resonances arise from protons on carbons alpha ($-CH_2-CH_2-COO^-$, 2.2 ppm) and beta ($-CH_2-CH_2-COO^-$, 1.6 ppm) to the carboxyl head group of the fatty acids. Further resonances from the glycerol backbone at 4.1 and 4.3 ppm are generally in regions of high spectral overlap, and are too weak to be observed, except under conditions of high lipid or lipid overload [13, 14] or alternately they can be detected by 2D MR techniques [15, 16]. 2D COSY spectra were originally used to demonstrate that the cross peaks from mobile lipids arise almost exclusively from neutral lipids, triglycerides and cholesterol esters [14, 15].

Origin of Mobile Lipids as Observed on ^{1}H MRS

Mobile lipids comprised of fatty acyl chains of triacylglycerides and cholesteryl esters have been detected by ^{1}H MRS in various cell types such as malignant transformed cells [17, 18], viral transformed cells [19], therapy induced transformed cells [16, 20] and activated immune cells (B and T cells, macrophages and neutrophils) [21-26]. Lipid resonances have also been observed *in vivo* in human cancers and are considered as important biomarkers in the diagnosis and monitoring the effects of treatment response [27, 28].

However, understanding the origin and subcellular location of these ^{1}H MR-visible mobile lipids has been a subject of debate with a focus on two alternative mechanisms. The first hypothesis proposes that mobile lipid signals originate from neutral lipids arranged in small isotropically tumbling microdomains (25-28 nm in diameter) embedded within the plasma membrane. This model is based on the similarity of MR spectra between whole cells and

isolated plasma membranes, the selective broadening of mobile lipid resonances by paramagnetic ions that do not cross the plasma membrane [17], the demonstration using selective T_1 relaxation experiments that the neutral lipids are not in diffusive exchange with bilayer lipids [29] and determination of elevated levels of neutral lipids in the plasma membrane that correlated with MR lipid visibility [30]. Subsequent studies showed that the differences observed in mobile lipid spectra were larger than could be accounted for changes by in lipid droplet number or diameter [31-33].

The second hypothesis attributes the presence of mobile lipids to the accumulation of lipid droplets in the cytoplasm of intact cells [34, 35] or their extracellular presence in the necrotic core of tumors [36-39]. Some investigators have considered a complementary role for both plasma membrane and intracellular compartments in contributing to MR-visible lipids [40]. Recent publications have proposed a unifying model that links changes in droplet size to alterations in the shuttling between plasma membrane phospholipids, endoplasmic reticulum and lipid droplets [41, 42].

In many instances, MR-visible lipid spectra are inducible by external stressful stimuli. In these cases, correlations have been shown between the formation of MR-visible lipids and cytoplasmic lipid droplets. Callies *et al.* [35] demonstrated that MR-visible lipid resonances were correlated with the formation of cytoplasmic lipid droplets when myeloma cells were grown in the presence of high concentrations of oleic acid. High extraneous lipid concentrations leading to the formation of MR-visible lipids was later shown in mixed peripheral blood lymphocytes and neutrophils by King *et al.* [24] and Wright *et al.* [21]. A number of studies showed similar accumulations of lipid droplets in response to low pH [43, 44] or treatment with cytotoxic or cytostatic drugs [2, 45-48]. Light and electron microscopy studies revealed these droplets to be micron-sized [2, 45-48], which was confirmed by measuring the restricted diffusion within the droplets using diffusion-weighted spectroscopy of the mobile methylene resonance [43].

These droplet sizes are in keeping with those measured in *in vivo* MR studies [49-51]. Hakumäki *et al.* [50, 51] reported the presence of intracellular lipid droplets (0.2- 2.0 μm) along with myeloid bodies in a malignant rat BT4C glioma undergoing herpes simplex virus thymidine kinase (HSV-*tk*)-mediated gene therapy. Studies on the C6 rat brain glioma model have shown that mobile lipids originate from triglyceride-containing lipid droplets (0.1-1.0 μm in diameter) in necrotic areas of the tumor [34]. Such accumulation of lipid droplets has also been observed by electron microscopy in necrotic areas of human brain tumor biopsies [52] and in animal tumors [53].

These data demonstrate that neutral lipids in cytoplasmic lipid droplets accumulate in response to external stimuli and are a major contributor to the mobile lipid signal detected by MRS. This is particularly relevant to this review, as condition of stress, such as those found in the tumor microenvironment, give rise to cytoplasmic mobile lipid droplets observable using MR.

Biology and biochemistry of the lipid droplet

The classic view of the lipid droplet is that it is an inert single membrane bound ball of neutral lipids that functions primarily as a storage dept for fatty acids. However, recent research has revealed that the lipid droplet is a dynamic organelle [54-56]. The formation of lipid droplets in adipocytes and other cell types is exquisitely controlled. Intracellular triglyceride synthesis takes place at the endoplasmic reticulum [57] and involves the condensation of an activated fatty acid (fatty acid-S-CoA) with diacylglycerol via the enzyme diacylglycerolacyltransferase. A similar intracellular reaction exists with acyl-CoA:cholesterol acyltransferase catalyzing cholesterol ester formation from free cholesterol

and a fatty acid. Lipid droplets are formed at the endoplasmic reticulum by budding, which creates an organelle with a neutral lipid core surrounded by a phospholipid monolayer. The PAT proteins, named after three of the main proteins in the family: perilipin, adipocyte differentiation related protein (ADRP) and tail interacting protein of 47 kDa (TIP47), are associated with the droplet surface and regulate trafficking of lipids into and out of the lipid droplet [58, 59].

The stress-induced formation of neutral lipids is poorly understood and most information comes from hepatocytes where the accumulation of intracellular triglyceride lipid droplets in the formation of fatty liver [13] been called "the harbinger of cell death" [60]. In stress-induced lipid droplet formation, neutral lipid droplet results from an oversupply of fatty acids and the compensatory shunting of these potentially toxic metabolites into lipid storage droplets, or even as a storage depot for certain proteins [61]. Recall that this is an energy consuming process as the synthesis of triglycerides and cholesterol esters requires ATP to activate the fatty acids. The oversupply of fatty acids can result from increased uptake of fatty acids from the extracellular milieu but there may also be contributions from decreased β-oxidation of fatty acids by the mitochondria or hydrolysis of membrane lipids induced by phospholipases [62] (see Figure 2). The relative contribution of each mechanism remains unknown and may vary between cell types, toxin and stress inducer.

Mobile Lipids and the Tumor Microenvironment

The tumor microenvironment consists of four components: cancer cells, non-cancer cells, secreted soluble factors and non-cellular solid materials including the extracellular matrix [63]. The relative contribution of each of these four components varies between tumor types, between patients with the same tumor, and even between regions of a single tumor. The tumor microenvironment will change over the course of tumor development and progression, and will alter in response to a therapeutic intervention. Many of the changes are controlled by physiological factors, for example the local degree of perfusion controlling the nutrient or oxygen levels within the tumor. This in turn leads to epigenetic adaptation, such as increases in HIF-1α levels in response to hypoxia, or secretion of vascular growth factors to stimulate new blood vessel growth. This local variability contributes to tumor heterogeneity, and the resulting genetic or epigenetic and physiological differences lead to relative differences in tumor growth, formation of hypoxic or necrotic regions within the tumor, and variation in drug resistance. With such a high-degree of variability, the ability to accurately and non-invasively monitor regional conditions or changes in the tumor microenvironment could provide information useful for tracking tumor progression or response to therapy if a suitable set of biomarkers could be determined and validated. Below we will explore the potential of using MRS to measure tumor environmental biomarkers, with emphasis on the mobile lipid profile. We will first consider the unique conditions generated within the tumor microenvironment and how these conditions may contribute to mobile lipid formation followed by discussion of the relevant cellular components within that environment.

Conducive conditions for mobile lipid formation within the tumor microenvironment

The tumor microenvironment is home to a number of harsh or undesirable conditions that are conducive for the formation of mobile lipids. Glucose and oxygen are depleted in poorly perfused regions of the tumor. This can occur when the tumor is large enough that the host's blood supply can no longer provide significant nutrients, even in the presence of increased angiogenesis. These conditions have profound effects on lipid metabolism that can be observed using MRS. Low extracellular pH results from products of the sugar and fat catabolism. In the absence of oxygen, the lactate anion is generated from glucose via pyruvate during glycolysis. Protons and NADH are generated in glycolysis by

glyceraldehyde-3-phosphate dehydrogenase and during three oxidative steps in the Krebs cycle. Carbonic acid arises from hydration of the CO_2 produced from the decarboxylation of α-ketoglutarate in the Krebs cycle. Lactate and associated protons are exported to the extracellular space via monocarboxylate transporters such as the lactate-proton co-transporter. Protons can be exported through a variety of transport systems including the sodium-proton exchanger, vacuolar H^+ adenosine triphosphatases, and the sodium-bicarbonate exchanger [64-66].

A variety of physiological, environmental and therapy-based conditions are known to influence the appearance of lipids in different cells, and these conditions are summarized in Table 2. It has been observed with ^{1}H MRS that the mobile lipid content of cultured tumor cells changes significantly during cell growth [16, 67]. An early study using transformed murine fibroblast cells showed that cell culture conditions, confluence, serum deprivation, and acidic extracellular pH could all induce the appearance of mobile lipids [16]. The increases in mobile lipids were accompanied by increases in polyunsaturated fatty acids (PUFA) and increases in GPC at the expense of PC, and the involvement of catabolic phospholipases was proposed (as demonstrated in Figure 2). The MR-visible lipid increases were linear below physiological pH and were also shown to be transient in nature. Barba *et al.* [44] showed that mobile lipids were barely visible in the log phase of cell growth in C6 glioma cells, but were clearly visible at saturation density. In their study, Nile red staining lipid droplets were present in 85% of cells at saturation density but only in 6% of the log phase cells [44, 68]. These investigators further showed that the low pH induced accumulation of mobile lipids is reversible. No direct studies on the effects of hypoxia on mobile lipid generation have been performed on cultured cells to our knowledge, but it has been known for some time that lipid droplets accumulate in hypoxic and necrotic regions of tumors [53]. Necrosis, however, will result in cell lysis, releasing a number of proteins, lipids and other small molecules into the extracellular milieu. We will show in the next sections that cultured cells that are sensitive to a number of toxins often respond by producing mobile lipids in the form of lipid droplets.

MR-Visible Lipids in Cell Models

Cancer Cells

A large percentage of the volume of any solid tumor consists of tumor cells. The tumor microenvironment varies across the diameter of a solid tumor contributing to tumor heterogeneity, and is modulated by the local conditions in the tumor. The local environment is further modulated by soluble factors, secreted cytokines, low pH caused by high levels of lactate and other small organic acids, and even fatty acids and other molecules secreted or released from hypoxic or necrotic cellular regions. The ^{1}H MR spectrum of tumor cells and of other contributing cell types can vary *in vitro* depending on culture conditions that mimic elements of the tumor microenvironment. Most notably, the level of mobile lipids can vary in an inducible and reproducible manner in response to chemical and other stresses, and thus we review this literature here using the paradigm of cell stress to approximate the tumor microenvironment.

It has been known for some time that tumor cells exposed to cytotoxic drugs exhibit increases in mobile lipids. An early demonstration of this phenomenon was in breast cancer cells treated with cationic lipophilic mitochondrial targeting drugs such as TPP and derivatives (Figure 1) [20, 69]. The mobile lipid accumulation was shown to be dependent on both exposure time and drug concentration and was accompanied by increases in GPC at the expense of PC. Electron and light microscopy revealed extensive mitochondrial damage and a time-dependent increase in cytoplasmic lipid droplets and endstage autophagic

vacuoles indicating lysosomal involvement [2, 47]. The increase in mobile lipids linearly correlated with the volume fraction of the cytoplasm occupied by lipid droplets [47, 70].

A number of studies have demonstrated an increase in mobile lipids that have been associated with the onset of drug-induced apoptosis. Increasing intensities of the CH_2/CH_3 ratio (the ratio of intensities from the methylene to methyl resonances at 1.3 and 0.9 ppm respectively) have been shown in Jurkat T lymphoblasts treated with anti-FAS antibodies [48], anthracycline antibiotics or glucocorticoid steroids [40, 71, 72], and in human erythroleukemia K562 cells by exposure to paclitaxel [73]. In cervical carcinoma cells the distinction between apoptosis, induced by the topoisomerase II inhibitor etoposide, and necrosis, induced by ethacrynic acid or cytochalasin B, could be made on the distinction of increased mobile lipids that occurred as early as 6 h after treatment [74]. In HL60 leukemia cells increases in the CH_2/CH_3 ratio after induction of apoptosis by ionizing radiation or by doxorubicin were accompanied by reductions in other MR-visible metabolites such as glutamine, glutamate, taurine, and glutathione [75]. On the other hand, heat-induced necrosis led to significant increases in all the aforementioned metabolites except glutathione with no observed increase in mobile lipids. The demonstration that MR-visible lipid could be induced in breast cancer cells by toxic concentrations of 5-fluorouracil, but not methotrexate, further indicated that this response is specific only to certain cytotoxic insults [70]. Moreover, at least one study has shown that the induction of mobile lipids is cell-cycle independent using a number of cell cycle blockers in normal and synchronized glioma cell populations [1]. More recently, BT-20 and MCF-7 cells treated with paclitaxel-loaded liposomes or micelles demonstrated increases in the fatty acyl resonance of the mobile lipids as the cells underwent apoptosis [76].

In prostate cancer cells treatment with the differentiating agents phenylacetate or phenylbutyrate (PB) led to accumulation of mobile lipids and tCho in ^{1}H spectra and GPC in ^{31}P spectra [45, 46, 77]. The onset of these changes occurred less than 2 h after treatment and was correlated with the presence of cytoplasmic lipid droplets (see Figure 3). The simultaneous increase in mobile lipids in the form of lipid droplets and GPC are indicative of the consecutive actions of phospholipase A2 (PLA2) and phospholipase A1 (PLA1) or lysophospholipase, each releasing a fatty acid that can be shunted into neutral lipids and forming GPC (Figure 2). Of note is that although both differentiating agents, phenylacetate and PB induce similar metabolic changes, the alterations are greater when the cells are treated with PB, which induces NTP loss and apoptosis, as opposed to phenylacetate, which induces only cytostasis.

Immune cells

Solid tumors contain a proportionately high number of infiltrating immune cells including neutrophils, macrophages and T and B lymphocytes. The roles of these immune cells in tumor development and progression remains to be fully determined and may include functions that are both beneficial and detrimental to tumor growth and survival. Importantly immune cells are often present in activated states and may provoke local inflammation. Moreover, many immune cells, including macrophages, are involved in the secretion of cytokines and other soluble factors that may modulate the tumor microenvironment and promote cell growth.

Of particular relevance to this article, the *in vitro* MR spectra of various immune cell populations have been characterized in quiescent and activated cells [17]. In isolated splenic or thymic T cells, mobile lipid accumulation is observed when these cells are activated by treatment with concanavalin A [78], the phorbol ester phorbol myristate acetate in the presence or absence of the calcium ionophore ionomycin [22, 23], or by engagement of the T cell receptor using anti-CD3 antibodies [79, 80]. In B cells, as well as in neutrophils, a

similar induction of mobile lipids can occur after stimulation with lipopolysaccharide [78]. In B and T cells, but not in neutrophils, the lipid changes are accompanied by the onset of proliferation [22, 23, 78]. It has further been shown that mobile lipid accumulation is not directly dependent on cell cycle, as treatment of T or B cells with cell cycle blockers such as nifedipene and desferrioxamine that inhibit proliferation before the G_1-S interface do not affect the onset or magnitude of the MR signal [26]. Treatment of mouse peritoneal macrophages with purified recombinant interferon-gamma (IFN-γ) leads to increased mobile lipid accumulation, as does systemic treatment of mice with *Listeria monocytogenes* followed by isolation of peritoneal macrophages [24, 25]. In human peripheral monocytes however IFN-γ does not cause mobile lipid accumulation [24]. Of particular interest is that terminally differentiated immune cells such as neutrophils and macrophages can be induced to accumulate mobile lipid not only by the use of stimulating agents, but also by exposure to high levels of serum or fatty acids (Figure 4), a condition likely to occur in anoxic or necrotic regions of the tumor microenvironment [21, 24]. Finally it is of interest to note that such metabolic changes may be transferable between cell types, as the co-culture of monocytes with autologous but unstimulated T-cells will cause mobile lipid accrual in the lymphocyte population with concomitant increases in cytoplasmic lipid droplets [81]. The mechanism of this phenomenon remains unclear, but it may be mediated through soluble factors or by intercellular contact or communication.

Fibroblasts

Host fibroblasts exist in tumors and are largely found in the stroma where they are the predominant cell types. Fibroblasts are involved in tumor progression, where they produce the proteolytic enzymes (matrix metalloproteinases) involved in the degradation of the extracellular matrix during the process of invasion.

Although MR spectroscopic studies are relatively few, there are some reports with fibroblasts or with transformed fibroblast cell lines. These cells, like other cell types, display variable amounts of mobile lipids depending on culture conditions and treatment. Rutter *et al.* demonstrated increases in mobile lipid accompanying extended *in vitro* passaging and or senescence in human fibroblast cultures [82]. As already described, harsh culture conditions, nutrient deprivation, simulated through over crowding by growth at high cell density, enhanced by serum removal, or by culture at low pH, contribute to the formation of increased mobile lipid in a transformed murine L cell line [16]. Low pH induced increases in mobile lipids were demonstrated to be transient following exposure of cells in log phase growth to culture medium at pH 6.1, indicating that cells employ compensatory mechanisms to deal with pH induced stress. The increase in MR-visible lipids was also shown in NIH-3T3 fibroblasts during serum starvation [72]. Other investigators have shown unexpectedly high mobile lipid signals in NIH-3T3 fibroblasts compared to their *ras*-transformed counterparts [83, 84]. Overall these studies indicate that accessory cells such as fibroblasts are capable of mobile lipid accumulation *in vitro* when exposed to a range of environmental or genetic stresses.

Factors Regulating Mobile Lipid Production

We have seen so far that mobile lipids can be inducible and can result from lipid overload or from treatment with cytostatic or cytotoxic drugs. Although mobile lipids can accompany the process of apoptotic, necrotic or autophagic cell death, mobile lipids are neither necessarily causative nor resultant of cell death, and therefore care must be taken when interpreting MR spectra. However, mobile lipids appear to be an early indicator of cell stress, preceding the committed decision of cell death.

A number of check points in the development of inducible mobile lipid signals have been identified in MR studies of isolated or perfused cells. First, triacsin C, a specific inhibitor of long-chain acyl-CoA synthetase was able to abolish MR-visible lipids and lipid body formation in a human lymphoblastoid cell line treated with anti-Fas monoclonal antibody, without affecting cell viability or inhibiting apoptosis [85]. In breast cancer cells, MR-visible lipids induced by cationic lipophilics could be prevented by pretreatment with chlorpromazine (see Figure 1), a lysomotropic agent that accumulates in acidic lysosomal compartments, increasing lysosomal pH and preventing autophagic digestion [2]. It was later shown that MR-visible lipid induced by the mitochondrial permeability transition inhibitor cyclosporin A or by the antimetabolite 5-fluorouracil in breast cancer cells could also be inhibited by chlorpromazine [86, 87], indicating a potentially common lysosomal mechanism involved in mobile lipid formation.

In the case of prostate tumor cells undergoing differentiation treatment with PB, the increases in tCho and GPC levels, but not mobile lipids could be enhanced by pre-treatment with the HMG-CoA reductase inhibitor lovastatin, even though the DNA fragmentation and the loss of NTP were reversed, signifying a metabolic branch point between lipid accumulation and the progression of apoptosis [45]. Furthermore both the spectroscopic (increases in MR-visible lipid, GPC and tCho, decreases in NTP) and biological (caspase activation, G_1 cell cycle arrest) effects of the differentiating agent PB could be prevented by pretreatment with the PPAR-γ antagonist GW9662 [77]. PPAR-γ is a ligand-activated transcription factor that has been shown to regulate the uptake and synthesis of triglycerides during adipocyte differentiation. Our recent data show that the spectroscopic effects of PB treatment can be attenuated using AACOCF3, an inhibitor of the high molecular weight phospholipases, iPLA2 and cPLA2 [88]. This is the first demonstration of increased PLA2 activity during mobile lipid formation. The involvement of PLA2 in mobile lipid generation in response to cytotoxic therapy was proposed in breast cancer and prostate cancer cells [20, 46]. This was followed by the demonstration of upregulation of an undetermined isoform of PLA2 in rat gliomas undergoing apoptosis in the HSV-*tk* model [89].

In summary, the majority of the data involving mobile lipids has come from studies involving isolated or perfused cells. These data have shown that MR-visible lipids can be induced by a number of stressful conditions similar to those that occur in the tumor microenvironment and in the cell types found in the tumor microenvironment, including tumor cells, activated immune cells and fibroblasts. Controlling factors regulating the accumulation of mobile lipids are beginning to emerge and the next few years should see significant advances in this field. The question that we will explore in the next two sections is whether such changes in lipid profiles can be observed in animal models and human tumors *in vivo*.

In vivo MRS of lipids in cancer

In order to perform MRS *in vivo*, spectral localization techniques are needed to detect metabolites from a region of interest. The most common localization techniques for single voxel spectroscopy include STEAM [90] and PRESS [91, 92]. Multi-voxel techniques include additional phase-encoding steps to provide spatial distribution of voxels and can be used in conjunction with STEAM or PRESS to provide anatomical localization. In order to detect MR-visible metabolites, which occur in the millimolar range, water suppression techniques are often applied, since the concentration of water protons in tissue is typically ~ 70 M. Additional lipid signals from adjacent subcutaneous fat, muscle, bone marrow or scalp need to be eliminated in order to observe the signals from the voxels of interest. These fat signals are typically suppressed by the use of frequency selective saturation pulses placed outside the region of interest [93]. While these techniques effectively suppress outer volume lipid signals in the brain, they are less effective on lipid signals in other organs due to the

overwhelming fat signal from adipose tissue in the breast, liver and prostate. This makes it more difficult to assess the MR lipid profile of these tumors *in vivo*.

The methyl (-CH$_3$) signal from lactate co-resonates with the methylene (-CH$_2$-C**H**$_2$-CH$_2$-) signals from mobile lipids at 1.3 ppm, and as such it is often difficult to separate the two moieties *in vivo*. In normal tissues, lactate signal is generally below detectable limits but in tumors the lactate concentration can be as high as 5-10 mM. Since mobile lipids have a much shorter relaxation time ($\sim$ 50 ms at 1.5 T) than lactate ($\sim$300 ms at 1.5 T), long echo time spectra are typically acquired to detect lactate while suppressing lipid signals. The lactate -CH$_3$ signal appears as an inverted doublet at an echo time of 136-144 ms in a spin-echo sequence due to modulation of the signal by the methyl to methine J coupling. Additional spectral editing sequences are often used to make a definite assignment between lactate and lipid signals, such as two-dimensional MR spectroscopy [15, 16, 20, 68, 70, 94, 95], homonuclear polarization transfer filters, and multiple quantum coherence (MQC) filters [96-98].

Suppressing lactate in order to selectively observe the lipid signal at 1.3 ppm is more difficult. However diffusion weighted MRS (DW-MRS), which integrates diffusion-sensitizing gradients into the MR pulse sequence to measure translational displacement of metabolites, has been employed to separate lactate from lipid components. Using DW-MRS, the apparent diffusion coefficient (ADC) of lactate was estimated to be $0.21\text{-}0.23 \times 10^{-9}$ m^2/s in an HMESO-1 tumor xenograft mouse model [99] and 0.12 to 0.18×10^{-9} m^2/s in a RG2 glioma in a rat [100]. Mobile lipids in lipid droplets experience restricted diffusion, and thus a lower ADC is observed ($0.046 \pm 0.017 \times 10^{-9}$ m^2/s for the 1.3 ppm resonance in a C6 rat brain glioma [34] and $0.063\pm0.013 \times 10^{-9}$ m^2/s in a B4TC glioma model [50]). This distinction has been used to suggest that contribution of lactate was negligible to the 1.3 ppm resonance in etoposide treated murine lymphoma tumors [95].

In vivo MRS of lipids in animal tumors

Spectroscopic studies on animal tumor models or human tumor xenografts exhibit similar lipid profiles as seen in cultured cancer cells. It has been reported that lipid signals are located in hypoxic / necrotic areas of the tumor, indicating that neutral lipids accumulate in response to these stresses *in vivo* [36, 37]. The confirmation of the intracellular nature of these lipid droplets comes from electron microscopy [34, 51]. Further evidence of the presence of lipid droplets inside intra-cranial C6 glioma tumors comes from diffusion spectroscopic studies using pulsed field gradient MRS [34]. The root mean square displacement of the protons contributing to the lipid resonance at 1.3 ppm was 2.6 ± 0.5 μm. These investigators further reported that a numbers of lipid droplets were localized in the necrotic center of the tumors in comparison to the peripheral regions [34]. In intra-cranial rat BT4C tumors, Hakumäki *et al.* [51] observed necrotic foci scattered throughout the tumor, however, the necrotic regions were more densely packed in the tumor core. These regions contained neutral lipids that stained positively with Sudan IV or oil red O [51]. Freitas *et al.* [53] demonstrated the presence of small necrotic foci on histological sections of solid Ehrlich carcinoma in mice as early as 9 days after tumor cell implantation. Nile red staining revealed the existence of lipid droplets in necrotic areas as well as in cells in the peripheral zone. After 12 days of tumor growth, necrotic areas were larger and lipid droplets were mainly found in these regions. The significance of the formation of intracellular lipid droplets is still poorly understood. However, recall that lipid droplets can represent a temporary storage compartment for fatty acids in the form of triglycerides, diacylglycerides or phospholipids. Under hypoxic or ischemic conditions, fatty acids may not be degraded by β-oxidation leading to lipid accumulation within the cell. As fatty acids are toxic to the cell, the cells sequester them as lipid droplets to avoid toxicity and as an alternative energy

source. Fatty acid oxidation has been shown to be a dominant pathway for energy production [101] and mice with pancreatic tumors fed on high fat diets showed increased lipid droplets and upregulation of medium-chain acyl–coenzyme A dehydrogenase expression, a regulator of fatty acid β-oxidation [102].

Changes in lipid signals in animal tumors in response to therapy

Mobile lipid resonances, especially the methyl and methylene peaks at 0.9 ppm and 1.3 ppm, are consistently observed in tumor cells and in animal tumor models indicating their potential as a diagnostic marker. However, a number of *in vivo* studies demonstrate increased mobile lipids in response to treatment during apoptosis and thus corroborate the *in vitro* studies. Initial evidence of changes in lipid signals in intracranial 9L tumors indicated a progressive increase in the lipid resonance at 1.3 ppm along with a decrease in choline and creatine resonances after fluoromethylene -2′-deoxycytidine treatment [103]. In this study, which was probably the first MR study of gene therapy in tumors, the authors reported increased MR-visible lipids after six days of intra-tumoral injection of adenoviral HSV-*tk* followed by ganciclovir treatment [103]. Later, using single voxel localization, Hakumäki et al. [50] reported accumulation of PUFA resonances at 2.8 and 5.3 ppm in intra-cranial BT4C glioma tumors expressing HSV-*tk* (see Figure 5). The presence of PUFA resonances correlated with regions of increased apoptosis within the tumor and this was later confirmed using magic angle spinning spectroscopy of excised tissues [104, 105]. Using ultra-short echo time chemical shift imaging, the spatial distribution of MR-visible lipids were mapped in this tumor model [106], demonstrating a temporal increase in saturated and unsaturated resonances that peaked 8 days after treatment (see Figure 6). It was suggested that the PUFA resonances arise from phospholipase A2 activity leading to hydrolysis of phosphatidylethanolamine in the cell membrane [89] and that some of the increase (~ 17%) in the terminal –CH_3 signal at 0.9 pm after induction of apoptosis could be explained by the increase in mobile cholesterol esters [107]. In line with these findings, Schmitz *et al.* observed increases in the 1.3 ppm methylene mobile lipid resonance in both isolated murine EL-4 lymphoma cells and solid tumors as an early event following etoposide-induced apoptosis [95]. In contrast to previous cell studies, these authors did not observe significant changes in the CH_2/CH_3 ratio either *in vitro* or *in vivo.* Recently, Lee *et al.* [49] observed increased saturated and unsaturated lipid resonances after radiation therapy in a subcutaneous human non-Hodgkin's diffuse large B-cell lymphoma xenograft. After 3 days of a single dose of 15 Gy radiation to the tumor, a dramatic increase in the PUFA resonance at 2.8 ppm was observed, which correlated with an increase in TUNEL positive cells and in oil red O positive perinuclear lipid droplets indicating that these organelles contributed to the observed MR spectrum (see Figure 7). These studies indicate that early increases in mobile lipid resonances after therapeutic intervention may be suggestive of apoptosis and positive treatment response. The temporal evolution of these resonances may be variable, with a decrease in lipid resonances during formation of scar tissue after cell death and lysis. It may be beneficial to include diffusion imaging experiments in conjunction with MRS experiments to accurately determine the physiological mechanisms in tumor response as reported recently [49, 106].

Ex vivo MRS of lipids in human tumors

As mentioned earlier, mobile lipid signals from subcutaneous fat, muscle and adipose tissue overlap substantially with intra-tumoral lipids and as such most *in vivo* MR studies of extra-cranial tumors do not focus on the utility of lipid resonances in cancer diagnosis and treatment response. However, several MR studies using *ex vivo* biopsy samples have been reported, where extraneous lipid from other tissues do not interfere with measurement of the MR-visible lipid profile. The original study on cervical biopsy specimens demonstrated the presence of mobile lipids in 39 out of 40 invasive carcinoma specimens but not in 119 punch

biopsy specimens of normal or preinvasive lesions [18]. At this time, it was proposed that MR-visible lipids were a potential marker of malignancy or malignant transformation [18, 108]. A number of subsequent studies recognized that MR-visible lipids occur at higher levels in spectra obtained from biopsies from ovary [109], prostate [110, 111] and thyroid [112, 113] tumors relative to those obtained from benign or normal tissues. Biopsies from both colon [114, 115] and breast [116] tissue showed high levels of MR-visible lipids regardless of diagnosis, but the distinction of malignant tissues could be made based on the presence of high tCho and other resonances. In breast biopsies, mobile lipids arise from normal fat present in the breast. In the colon it was originally demonstrated [115] and then elegantly shown using chemical shift imaging that MR-visible lipids in normal colon arise from the submucosa, where numerous oil red O lipid droplets were observed resulting from lipid resorption or from macrophages [117]. This observation was also confirmed in rat colon carcinoma tissues [118]. In a series of papers on brain tumor biopsies, Kuesel *et al.* demonstrated a correlation between necrosis and MR-visible lipid signal intensity, especially with regard to the unsaturated resonance at 5.3 ppm [36, 37, 119]. They also showed that the MR-visible lipid signal could vary significantly in samples with 0–5% necrosis and attributed this to metabolic heterogeneity within a biopsy sample [36]. These studies were the first to link MR-visible lipids to necrosis and give credence to the hypothesis that the mobile lipids appearing in tumor tissue may result from the ischemic conditions in the tumor microenvironment.

The introduction of biological magic angle spinning MRS has brought renewed interest in the study of biopsy tissue specimens. Magic angle spinning studies have revealed a number of resonances with potential diagnostic or biochemical significance that were not visible or could not be resolved using non-spinning techniques. However, in the majority of studies where mobile lipids are discussed directly, the general observations made above still hold, that mobile lipids are increased in biopsy specimens from malignant tissues. A number of magic angle spinning studies have reported increased MR-visible lipid spectra in cervical cancer biopsies relative to premalignant tissues [120-123]. Apoptotic cell density was shown to correlate with the CH_2 / CH_3 ratio in pulse-acquire but not in spin-echo magic angle spectra of cervical carcinoma specimens [124]. Further, Zietkowski *et al.* utilized diffusion-weighted magic angle spinning to show increased polyunsaturated lipids in cervical carcinoma biopsies [125] and increased PUFA were also observed in a subgroup of prostate cancer tumors [126]. A strong correlation between Nile red-positive droplets and the 1.3 ppm peak of MR-visible lipids was found in astrocytoma biopsies [127]. In non-necrotic regions the number of lipid droplets correlated with cell density, whereas in necrotic regions they correlated with percentage necrosis. This provides further evidence that the formation of cytoplasmic MR-visible lipid signals is stress-induced markers that precede necrosis. In cervical cancer [123] and in astrocytoma biopsies [128] a good correlation was observed between *in vivo* and *ex vivo* spectra, indicating the MR-visible lipids are not an artifact due to sample processing.

In vivo MRS of lipids in brain tumor diagnosis

As most lipids in the normal brain are contained in bilayer membranes, *in vivo* MRS studies of the normal brain do not exhibit mobile lipid resonances. However, in most brain tumors, increased mobile lipid resonances are commonly observed when the spectra are acquired with echo times shorter than 50 ms. Similar to the observations in cancer cells and animal tumor models, brain tumor spectra typically exhibit increased lipid resonances at 0.9 and 1.3 ppm, however the unsaturated resonances at 2.8 and 5.3 ppm are often below detectable limits. Mobile lipid resonances are generally observed in contrast enhancing regions as well as necrotic areas of the tumor. In general, brain tumors are highly heterogeneous and include areas of viable tumor, necrosis and hemorrhage. Tumor malignancy or grading is often used

for prognosis and therapeutic management and the presence of necrosis on histological sections indicates malignancy based on the WHO classification of tumors. In an early publication, Poptani *et al.* reported that solid high-grade gliomas exhibited higher Cho/Cr ratio and increased mobile lipids in comparison to low-grade gliomas [129]. These authors later demonstrated that elevated lipid resonances were a characteristic of high grade gliomas even in cystic neoplasms, where the Cho/Cr or Cho/NAA ratio failed to predict the degree of malignancy of the tumor [130]. Several research groups have replicated these early *in vivo* findings over the years [131-135] indicating the important role of MR-visible lipids in brain tumor diagnosis. An additional important clinical question in space-occupying lesions of the brain is the accurate differential diagnosis of gliomas from lymphomas and brain metastases. These issues are dealt with in the sections below.

Differential Diagnosis of Brain Metastases and Identification of Their Primary Site

Glioblastomas originate from glial cells and infiltrate into normal brain tissue whereas metastases are generally encapsulated and disseminate from the primary neoplasms and invade into the brain by the hematogenous route. Because of their different cellular origins, it has been hypothesized that glioblastomas and metastases might have different metabolism that may be distinguished through their lipid profile. Opstad *et al.* [136] observed a significantly higher lipid peak area ratio (1.3 / 0.9 ppm) in metastases compared to glioblastomas from the solid portion of the neoplasms demonstrating the utility of ^{1}H MRS in distinguishing glioblastomas from metastases. Recently we have shown that MR spectra from peritumoral regions of gliomas show increased lipid resonances in comparison to the peritumoral regions in metastases indicating the invasive nature of gliomas [137]. In addition to the differential diagnosis of brain metastases, identification of the primary cancer site is also crucial as prognosis and survival of these patients depends on the location of the primary cancer. It has been reported that lipids play an important role in characterization of primary cancers in patients with brain metastases. Using principle component analysis of the lipid profile, Sjobakk *et al.* [138] observed that brain metastases from primary lung and breast cancer were separated into two clusters based upon the lipid resonances at 0.9 and 1.3 ppm, while metastases from malignant melanomas showed no uniformity. In another study, it was observed that metastases from colorectal carcinoma were dominated by strong lipid signals and showed higher scores of principle component 1 (characterized by lipid signals at 0.91, 1.30, 1.59, 2.03 and 2.26 ppm) compared to metastases of other origins. Higher mobile lipid levels in colorectal carcinoma metastases were attributed to relatively greater presence of coagulation necrosis [139].

Differential Diagnosis of Lymphomas

Primary cerebral lymphomas (PCLs) are primarily B cell non-Hodgkin's lymphomas that are hypercellular in nature and comprised of lymphoid cells and macrophages [140]. These tumors are highly homogenous in nature and exhibit strong contrast enhancement on MRI. Unlike gliomas, PCLs do not generally exhibit areas of necrosis, however, a characteristic metabolite pattern including the presence of highly elevated lipid levels from the solid and enhancing portion of the neoplasms is diagnostic of PCLs especially in immunocompetent patients [141-143]. High lipid levels in these tumors (in the absence of necrosis) may be due to the presence of activated or transformed lymphocytes or macrophages, since these cell types can contain high levels of MR-visible lipids [24, 25]. It has also been reported that ^{1}H MRS from the contrast enhancing regions can differentiate PCLs from high-grade gliomas as PCLs demonstrate higher Cho and lipid levels [141]. Like high-grade gliomas, an abnormal metabolite pattern has also been observed from regions outside the contrast enhancement in PCLs suggesting the presence of infiltrative active lymphocytes and macrophages in the peritumoral regions [137, 144] (see Figure 8). It is to be noted though that unlike glioblastomas, PCLs are angiocentric neoplams, and form perivascular cuffs of

tumor cells and infiltrate brain parenchyma either as individual diffusely infiltrating cells or as compact aggregates of tightly packed cells [140].

MR visible lipids in response to radiation therapy

While the role of MR-visible lipids in diagnosis and grading of tumors is being recognized in clinical studies of brain neoplasms, its role in monitoring treatment response has not been extensively studied despite several promising results in animal tumor models that show an increase in mobile lipids after therapy [49, 95, 106]. This may be due to the presence of spontaneous necrosis in gliomas and metastatic tumors, which also exhibit increased lipids. Nevertheless, a progressive increase in lipid resonances at 0.9 and 1.3 ppm was reported in a brain tumor patient up to 5 months after radiation therapy [145]. While the increased lipid resonances were hypothesized to be due to activated macrophages, it may also have been due to radiation-induced necrosis. Multivoxel MRS and image guided biopsy of malignant gliomas following chemo-radiotherapy was able to distinguish pure tumor tissue from necrosis on the basis of high tCho/Cr and low lipid+lactate/tCho [146]. A decrease in tCho, disappearance of lactate and an increase in mobile lipids was observed in patients with brain metastases for up to 1 month after treatment with stereotactic gamma knife surgery [147]. The inclusion of advanced MRI techniques such as perfusion weighted imaging [148, 149] and diffusion weighted imaging [150] may further assist in the differentiation of tumor recurrence from radiation necrosis. A multiparametric approach that includes MRI and MRS may prove to be more accurate in differentiating these two entities.

Summary and Conclusions

Mobile lipids or MR-visible lipids are triglycerides and cholesterol esters that accumulate in lipid droplets and have been observed in tumor cells, animal tumor models and in human tumors. They often arise in response to harsh or unfavorable conditions in culture or *in situ* but can also occur in response to anticancer drug treatment as an early marker in the process of apoptosis. Mobile lipids can be stress induced and in these cases, primarily arise from intracellular lipid droplets, but may also occur from lipid droplets that have leaked out from damaged cells in necrotic areas. However, the presence of tumoral MR-visible lipids may not only be due to tumor cells. Contributions from accessory cells such as immune cells and fibroblasts are also possible and there is still no effective way to distinguish this *in vivo*. A number of issues remain in delineating tumor mobile lipid signals from those that are constitutively present in normal tissues such as subcutaneous fat, and this makes it difficult to define specificity of mobile lipid resonances *in vivo*. However, studies in tumor models are beginning to determine the regulatory factors controlling mobile lipid production, and this comes at a time where the lipid droplet is increasingly being recognized as an important functional organelle and not simply an inert bag of cytoplasmic fat. In conjunction with improvements in imaging technology that allow increased signal to noise and spectral resolution at higher fields, we expect the discovery of many aspects of MR-visible lipid biology to occur over the next few years. It is hoped that this will provide critical information in the understanding of tumor progression and development and further prove to be clinically useful in diagnosis and staging of human tumors.

Acknowledgments

References

1. Delikatny EJ, Jeitner TM. The accumulation of ^{1}H MR-visible lipid in human glioma cells is independent of the cell cycle. Int J Oncol. 1997; 11:543–550. [PubMed: 21528245]

2. Sathasivam N, Brammah S, Wright LC, Delikatny EJ. Inhibition of tetraphenylphosphonium-induced NMR-visible lipid accumulation in human breast cells by chlorpromazine. Biochim Biophys Acta. 2003; 1633:149–160. [PubMed: 14499734]

3. Lei H, Poitry-Yamate C, Preitner F, Thorens B, Gruetter R. Neurochemical profile of the mouse hypothalamus using in vivo 1H MRS at 14.1 T. NMR Biomed. 2010; 23:578–583. [PubMed: 20235335]

4. Tkac I, Henry PG, Andersen P, Keene CD, Low WC, Gruetter R. Highly resolved in vivo 1H NMR spectroscopy of the mouse brain at 9.4T. Magn Reson Med. 2004; 52:478–484. [PubMed: 15334565]

5. Tkac I, Oz G, Adriany G, Ugurbil K, Gruetter R. In vivo 1H NMR spectroscopy of the human brain at high magnetic fields: metabolite quantification at 4T vs. 7T. Magn Reson Med. 2009; 62:868–879. [PubMed: 19591201]

6. Glunde K, Jie C, Bhujwalla ZM. Molecular causes of the aberrant choline phospholipid metabolism in breast cancer. Cancer Res. 2004; 64:4270–4276. [PubMed: 15205341]

7. Podo F. Tumour phospholipid metabolism. NMR Biomed. 1999; 12:413–439. [PubMed: 10654290]

8. Williams E, Hamilton JA, Jain MK, Allerhand A, Cordes EH, Ochs S. Natural abundance carbon-13 nuclear magnetic resonance spectra of the canine sciatic nerve. Science. 1973; 181:869–871. [PubMed: 4724077]

9. Mountford CE, Mackinnon WB, Russell P, Rutter A, Delikatny EJ. Human cancers detected by proton MRS and chemical shift imaging *ex vivo*. Anticancer Res. 1996; 16:1521–1531. [PubMed: 8694521]

10. de Certaines JD, Le Moyec L, Sequin F, Eliat PA, Constans JM. Nuclear Magnetic Resonance Spectroscopy of Lipids in Cancer. Current Organic Chemistry. 2007; 11:529–546.

11. Hakumäki JM, Kauppinen RA. 1H NMR visible lipids in the life and death of cells. Trends Biochem Sci. 2000; 25:357–362. [PubMed: 10916153]

12. Mountford CE, Doran S, Lean CL, Russell P. Proton MRS can determine the pathology of human cancers with a high level of accuracy. Chem Rev. 2004; 104:3677–3704. [PubMed: 15303833]

13. Corbin IR, Furth EE, Pickup S, Siegelman ES, Delikatny EJ. In vivo assessment of hepatic triglycerides in murine non-alcoholic fatty liver disease using magnetic resonance spectroscopy. Biochim Biophys Acta. 2009; 1791:757–763. [PubMed: 19269347]

14. Holmes KT, Mountford CE. Identification of triglyceride in malignant cell membranes. J Magn Reson. 1991; 93:407–409.

15. Cross KJ, Holmes KT, Mountford CE, Wright PE. Assignment of acyl chain resonances from membranes of mammalian cells by two-dimensional NMR methods. Biochemistry. 1984; 23:5895–5897. [PubMed: 6525339]

16. Delikatny EJ, Lander CM, Jeitner TM, Hancock R, Mountford CE. Modulation of MR-visible mobile lipid levels by cell culture conditions and correlations with chemotactic response. Int J Cancer. 1996; 65:238–245. [PubMed: 8567123]

17. Mountford CE, Grossman G, Reid G, Fox RM. Characterization of transformed cells and tumours by proton nuclear magnetic resonance spectroscopy. Cancer Res. 1982; 42:2270–2276. [PubMed: 6280854]

18. Delikatny EJ, Russell P, Hunter JC, Hancock R, Atkinson K, van Haaften-Day C, Mountford CE. Proton MR and cervical neoplasia: *Ex vivo* spectroscopy allows distinction of invasive carcinoma of the cervix from carcinoma *in situ* and other preinvasive lesions. Radiology. 1993; 188:791–796. [PubMed: 8351349]

19. Nicolau C, Dietrich W, Steiner MR, Steiner S, Melnick JL. [1]H and ^{13}C nuclear magnetic resonance spectra of the lipids in normal and SV 40 virus-transformed hamster embryo fibroblast membranes. Biochim Biophys Acta. 1975; 382:311–321. [PubMed: 1168502]

20. Delikatny EJ, Roman SK, Hancock R, Jeitner TM, Lander CM, Rideout DC, Mountford CE. Tetraphenylphosphonium chloride induced MR-visible lipid accumulation in a malignant human breast cell line. Int J Cancer. 1996; 67:72–79. [PubMed: 8690528]

21. Wright LC, Groot Obbink KL, Delikatny EJ, Santangelo RT, Sorrell TC. The origin of ^{1}H NMR-visible triacylglycerol in human neutrophils: high fatty acid environments result in preferential sequestration of palmitic acid into plasma membrane triacylglycerol. Eur J Biochem. 2000; 267:68–78. [PubMed: 10601852]

22. Dingley AJ, King NJC, King GF. An NMR investigation of the changes in plasma membrane triglyceride and phospholipid precursors during the activation of T-lymphocytes. Biochemistry. 1992; 31:9098–9106. [PubMed: 1390696]

23. Dingley AJ, Veale MF, King NJC, King GF. Two-dimensional ^{1}H NMR studies of membrane changes during the activation of primary T-lymphocytes. Immunomethods. 1994; 4:127–138. [PubMed: 8069532]

24. King NJC, Delikatny EJ, Holmes KT. [1]H Magnetic resonance spectroscopy of primary human and murine cells of the myeloid lineage. Immunomethods. 1994; 4:188–198. [PubMed: 8069537]

25. King NJC, Ward MH, Holmes KT. Magnetic resonance studies of murine macrophages: Proliferation is not a prerequisite for acquisition of an "activated" high resolution spectrum. FEBS Lett. 1991; 287:97–101. [PubMed: 1908793]

26. Holmes KT, Lean CL, Hunt NH, King NJC. Development of the "activated" high-resolution ^{1}H MR spectrum in murine T-cells and B-cells occurs in G_1 phase of cell cycle. Magn Reson Med. 1990; 16:1–8. [PubMed: 2255232]

27. Lindskog M, Spenger C, Klason T, Jarvet J, Graslund A, Johnsen JI, Ponthan F, Douglas L, Nordell B, Kogner P. Proton magnetic resonance spectroscopy in neuroblastoma: current status, prospects and limitations. Cancer Lett. 2005; 228:247–255. [PubMed: 15946794]

28. Sibtain NA, Howe FA, Saunders DE. The clinical value of proton magnetic resonance spectroscopy in adult brain tumours. Clin Radiol. 2007; 62:109–119. [PubMed: 17207692]

29. Mountford CE, Mackinnon WB, Bloom M, Burnell EE, Smith ICP. NMR methods for characterising the state of the surfaces of complex mammalian cells. J Biochem Biophys Methods. 1984; 9:323–330. [PubMed: 6491154]

30. Mackinnon WB, May GL, Mountford CE. Esterified cholesterol and triglyceride are present in plasma membranes of Chinese hamster ovary cells. Eur J Biochem. 1992; 205:827–839. [PubMed: 1572374]

31. Le Moyec L, Millot G, Tatoud R, Calvo G, Eugène M. Lipid signals detected by NMR proton spectroscopy of whole cells are not correlated to lipid droplets evidenced by the Nile red staining. Cell Mol Biol. 1997; 43:703–709. [PubMed: 9298592]

32. Mackinnon WB, Dyne M, Holmes KT, Mountford CE, Gupta RS. Further evidence that the narrow ^{1}H magnetic resonance signals from malignant cells do not arise from intracellular lipid droplets. NMR in Biomed. 1989; 2:161–164.

33. May GL, Sztelma K, Sorrell TC. The presence of cytoplasmic lipid droplets is not sufficient to account for neutral lipid signals in the 1H MR spectra of neutrophils. Magn Reson Med. 1994; 31:212–217. [PubMed: 8133757]

34. Rémy C, Fouilhé N, Barba I, Sam-Laï E, Lahrech H, Cucurella MG, Izquierdo M, Moreno A, Ziegler A, Massarelli R, Décorps M, Arús C. Evidence that mobile lipids detected in rat brain glioma by H1 nuclear magnetic resonance correspond to lipid droplets. Cancer Res. 1997; 57:407–414. [PubMed: 9012466]

35. Callies R, Sri-Pathmanathan RM, Ferguson DYP, Brindle KM. The appearance of neutral lipid signals in the ^{1}H NMR spectra of a myeloma cell line correlates with the induced formation of cytoplasmic lipid droplets. Magn Reson Med. 1993; 29:546–550. [PubMed: 8464371]

36. Kuesel AC, Donnelly SM, Halliday W, Sutherland GR, Smith ICP. Mobile lipids and metabolic heterogeneity of brain tumours as detectable by *ex vivo* [1]H MR spectroscopy. NMR Biomed. 1994; 7:172–180. [PubMed: 7946995]

37. Kuesel AC, Sutherland GR, Halliday W, Smith ICP. ^{1}H MRS of high grade astrocytomas: mobile lipid accumulation in necrotic tissue. NMR Biomed. 1994; 7:149–155. [PubMed: 8080717]

38. Zoula S, Herigault G, Ziegler A, Farion R, Decorps M, Remy C. Correlation between the occurrence of 1H-MRS lipid signal, necrosis and lipid droplets during C6 rat glioma development. NMR Biomed. 2003; 16:199–212. [PubMed: 14558118]

39. Lahrech H, Zoula S, Farion R, Rémy C, Décorps M. *In vivo* measurement of the size of lipid droplets in an intracerebral glioma in the rat. Magn Reson Med. 2001; 45:409–414. [PubMed: 11241697]

40. Di Vito M, Lenti L, Knijn A, Iorio E, D'Agostino F, Molinari A, Calcabrini A, Stringaro A, Meschini S, Arancia G, Bozzi A, Strom R, Podo F. 1H NMR-visible mobile lipid domains correlate with cytoplasmic lipid bodies in apoptotic T-lymphoblastoid cells. Biochim Biophys Acta. 2001; 1530:47–66. [PubMed: 11341958]

41. Quintero M, Cabanas ME, Arus C. 13C-labelling studies indicate compartmentalized synthesis of triacylglycerols in C6 rat glioma cells. Biochim Biophys Acta. 2010; 1801:693–701. [PubMed: 20380892]

42. Quintero M, Cabanas ME, Arus C. A possible cellular explanation for the NMR-visible mobile lipid (ML) changes in cultured C6 glioma cells with growth. Biochim Biophys Acta. 2007; 1771:31–44. [PubMed: 17150408]

43. Perez Y, Lahrech H, Cabanas ME, Barnadas R, Sabes M, Remy C, Arus C. Measurement by nuclear magnetic resonance diffusion of the dimensions of the mobile lipid compartment in C6 cells. Cancer Res. 2002; 62:5672–5677. [PubMed: 12384523]

44. Barba I, Cabañas ME, Arús C. The relationship between nuclear magnetic resonance-visible lipids, lipid droplets, and cell proliferation in cultured C6 cells. Cancer Res. 1999; 59:1861–1868. [PubMed: 10213493]

45. Milkevitch M, Jeitner TM, Beardsley N, Delikatny EJ. Lovastatin enhances phenylbutyrate-induced MR-visible glycerophosphocholine but not apoptosis in DU145 prostate cells. Biochimica Biophysica Acta. 2007; 1771:1166–1176.

46. Milkevitch M, Shim H, Pilatus U, Pickup S, Wehrle JP, Samid D, Poptani H, Glickson JD, Delikatny EJ. Increases in NMR visible lipid and glycerophosphocholine during phenylbutyrate-induced apoptosis in human prostate cancer cells. Biochimica Biophysica Acta. 2005; 1734:1–12.

47. Delikatny EJ, Cooper WA, Brammah S, Sathasivam N, Rideout DC. Nuclear magnetic resonance-visible lipid induced by cationic lipophilic chemotherapeutic agents are accompanied by increased lipid droplet formation and damaged mitochondria. Cancer Res. 2002; 62:1394–1400. [PubMed: 11888911]

48. Al-Saffar NM, Titley JC, Robertson D, Clarke PA, Jackson LE, Leach MO, Ronen SM. Apoptosis is associated with triacylglycerol accumulation in Jurkat T-cells. Brit J Cancer. 2002; 86:963–970. [PubMed: 11953830]

49. Lee SC, Poptani H, Pickup S, Jenkins WT, Kim S, Koch CJ, Delikatny EJ, Glickson JD. Early detection of radiation therapy response in non-Hodgkin's lymphoma xenografts by in vivo 1H magnetic resonance spectroscopy and imaging. NMR Biomed. 2010; 23:624–632. [PubMed: 20661875]

50. Hakumäki JM, Poptani H, Sandmair AM, Ylä-Herttuala S, Kauppinen RA. ^{1}H MRS detects polyunsaturated fatty acid accumulation during gene therapy of glioma: Implications for the *in vivo* detection of apoptosis. Nat Med. 1999; 5:1323–1327. [PubMed: 10546002]

51. Hakumaki JM, Poptani H, Puumalainen AM, Loimas S, Paljarvi LA, Yla-Herttuala S, Kauppinen RA. Quantitative 1H nuclear magnetic resonance diffusion spectroscopy of BT4C rat glioma during thymidine kinase-mediated gene therapy in vivo: identification of apoptotic response. Cancer Res. 1998; 58:3791–3799. [PubMed: 9731486]

52. Martinez-Perez I, Moreno A, Barba I, Capdevila A, Arus C. Large lipid droplets observed by electron microscopy in six human brain tumors with lipid 1H MRS in vivo pattern. Proc Intl Soc Magn Reson Med. 1996; 4

53. Freitas I, Pontiggia P, Barni S, Bertone V, Parente M, Novarina A, Roveta G, Gerzeli G, Stoward P. Histochemical probes for the detection of hypoxic tumour cells. Anticancer Res. 1990; 10:613–622. [PubMed: 1695078]

54. Martin S, Parton RG. Lipid droplets: a unified view of a dynamic organelle. Nat Rev Mol Cell Biol. 2006; 7:373–378. [PubMed: 16550215]

55. Olofsson SO, Bostrom P, Andersson L, Rutberg M, Perman J, Boren J. Lipid droplets as dynamic organelles connecting storage and efflux of lipids. Biochim Biophys Acta. 2009; 1791:448–458. [PubMed: 18775796]

56. Murphy DJ. The biogenesis and functions of lipid bodies in animals, plants and microorganisms. Prog Lipid Res. 2001; 40:325–438. [PubMed: 11470496]

57. Ohsaki Y, Cheng J, Suzuki M, Shinohara Y, Fujita A, Fujimoto T. Biogenesis of cytoplasmic lipid droplets: from the lipid ester globule in the membrane to the visible structure. Biochim Biophys Acta. 2009; 1791:399–407. [PubMed: 18996222]

58. Bickel PE, Tansey JT, Welte MA. PAT proteins, an ancient family of lipid droplet proteins that regulate cellular lipid stores. Biochim Biophys Acta. 2009; 1791:419–440. [PubMed: 19375517]

59. Robenek H, Buers I, Hofnagel O, Robenek MJ, Troyer D, Severs NJ. Compartmentalization of proteins in lipid droplet biogenesis. Biochim Biophys Acta. 2009; 1791:408–418. [PubMed: 19118639]

60. Cotran, RS.; Kumar, V.; Robbins, SL. Pathologic Basis of Disease. 4th. W.B. Saunders Co; Philadelphia: 1989.

61. Welte MA. Proteins under new management: lipid droplets deliver. Trends Cell Biol. 2007; 17:363–369. [PubMed: 17766117]

62. Gubern A, Barcelo-Torns M, Casas J, Barneda D, Masgrau R, Picatoste F, Balsinde J, Balboa MA, Claro E. Lipid droplet biogenesis induced by stress involves triacylglycerol synthesis that depends on group VIA phospholipase A2. J Biol Chem. 2009; 284:5697–5708. [PubMed: 19117952]

63. Cretu A, Brooks PC. Impact of the non-cellular tumor microenvironment on metastasis: potential therapeutic and imaging opportunities. J Cell Physiol. 2007; 213:391–402. [PubMed: 17657728]

64. Gatenby RA, Smallbone K, Maini PK, Rose F, Averill J, Nagle RB, Worrall L, Gillies RJ. Cellular adaptations to hypoxia and acidosis during somatic evolution of breast cancer. Br J Cancer. 2007; 97:646–653. [PubMed: 17687336]

65. Zhang X, Lin Y, Gillies RJ. Tumor pH and its measurement. J Nucl Med. 2010; 51:1167–1170. [PubMed: 20660380]

66. Voet, D.; Voet, JG. Biochemistry. 3rd. John Wiley and Sons; New York: 2004.

67. Le Moyec L, Tatoud R, Eugène M, Gauvillé C, Primot I, Charlemagne D, Calvo F. Cell and membrane lipid analysis by proton magnetic resonance spectroscopy in five breast cancer cell lines. Br J Cancer. 1992; 66:623–628. [PubMed: 1329906]

68. Barba I, Mann P, Cabañas ME, Arús C, Gasparovic C. Mobile lipid production after confluence and pH stress in perfused C6 cells. NMR Biomed. 2001; 14:33–40. [PubMed: 11252038]

69. Roman SK, Jeitner TM, Hancock R, Cooper WA, Rideout DC, Delikatny EJ. Induction of magnetic resonance-visible lipid in a transformed human breast cell line by tetraphenylphosphonium chloride. Int J Cancer. 1997; 73:570–579. [PubMed: 9389574]

70. Cooper WA, Bartier WA, Rideout DC, Delikatny EJ. 1H NMR visible lipids are induced by phosphonium salts and 5-fluorouracil in human breast cancer cells. Magn Reson Med. 2001; 45:1001–1010. [PubMed: 11378877]

71. Blankenberg FG, Katsikis PD, Storrs RW, Beaulieu C, Spielman D, Chen JY, Naumovski L, Tait JF. Quantitative analysis of apoptotic cell death using proton nuclear magnetic resonance spectroscopy. Blood. 1997; 89:3778–3786. [PubMed: 9160684]

72. Blankenberg FG, Storrs RW, Naumovski L, Goralski T, Spielman D. Detection of apoptotic cell death by proton nuclear magnetic resonance spectroscopy. Blood. 1996; 87:1951–1956. [PubMed: 8634443]

73. Brisdelli F, Iorio E, Knijn A, Ferretti A, Marcheggiani D, Lenti L, Strom R, Podo F, Bozzi A. Two-step formation of 1H NMR visible mobile lipids during apoptosis of paclitaxel-treated K562 cells. Biochem Pharmacol. 2003; 65:1271–1280. [PubMed: 12694868]

74. Bezabeh T, Mowat MRA, Jarolim L, Greenberg AH, Smith ICP. Detection of drug-induced apoptosis and necrosis in human cervical carcinoma cells using ^{1}H NMR spectroscopy. Cell Death Differ. 2001; 8:219–224. [PubMed: 11319604]

75. Rainaldi G, Romano R, Indovina P, Ferrante A, Motta A, Indovina PL, Santini MT. Metabolomics using 1H-NMR of apoptosis and Necrosis in HL60 leukemia cells: differences between the two

types of cell death and independence from the stimulus of apoptosis used. Radiat Res. 2008; 169:170–180. [PubMed: 18220461]

76. Musacchio T, Toniutti M, Kautz R, Torchilin VP. 1H NMR detection of mobile lipids as a marker for apoptosis: the case of anticancer drug-loaded liposomes and polymeric micelles. Mol Pharm. 2009; 6:1876–1882. [PubMed: 19737025]

77. Milkevitch M, Beardsley NJ, Delikatny EJ. Phenylbutyrate induces apoptosis and lipid accumulations via a peroxisome proliferator-activated receptor gamma-dependent pathway. NMR Biomed. 2010; 23:473–479. [PubMed: 20225233]

78. Holmes KT, Williams PG, Bloom M, Dyne M, Mountford CE, King N, Karaman M, Ninham B, Blanden R. Magnetic resonance study of lymphocytes stimulated with concanavalin A. Magn Reson Med Biol. 1988; 1:75–79.

79. Veale MF, Dingley AJ, King GF, King NJC. 1H-NMR visible neutral lipids in activated T lymphocytes: relationship to phosphatidylcholine cycling. Biochim Biophys Acta. 1996; 1303:215–221. [PubMed: 8908156]

80. Veale MF, Roberts NJ, King GF, King NJC. The generation of 1H-NMR-detectable mobile lipid in stimulated lymphocytes: relationship to cellular activation, the cell cycle, and phosphatidyl-choline specific phospholipase C. Biochem Biophys Res Commun. 1997; 239:868–874. [PubMed: 9367861]

81. Delikatny EJ, van Holst Pellekaan CJ, NJC King. Autologous lymphocyte-monocyte co-culture increases NMR-visible and cytoplasmic lipids in the absence of increased markers of lymphocyte activation. Biochimica Biophysica Acta. 2001; 1533:243–254.

82. Rutter A, Mackinnon W, Huschtscha L, Mountford CE. A proton magnetic resonance spectroscopy study of ageing and transformed human lung fibroblasts. Exp Gerontol. 1996; 31:669–686. [PubMed: 9415096]

83. Ferretti A, Knijn A, Iorio E, Pulciani S, Gaimbenedetti M, Molinari A, Meschini S, Stringaro A, Calcabrini A, Freitas I, Strom R, Arancia G, Podo F. Biophysical and structural characterization of 1H-NMR-detectable mobile lipid domains in NIH-3T3 fibroblasts. Biochim Biophys Acta. 1999; 1438:329–348. [PubMed: 10366776]

84. Knijn A, Ferretti A, Zhang PJ, Giambenedetti M, Molinari A, Meschini S, Pulciani S, Podo F. Lower levels of 1H MRS-visible mobile lipids in H-ras transformed tumorigenic fibroblasts with respect to their untransformed parental cells. Cell Mol Biol (Noisy-le-grand). 1997; 43:691–701. [PubMed: 9298591]

85. Iorio E, Di Vito M, Spadaro F, Ramoni C, Lococo E, Carnevale R, Lenti L, Strom R, Podo F. Triacsin C inhibits the formation of 1H NMR-visible mobile lipids and lipid bodies in HuT 78 apoptotic cells. Biochim Biophys Acta. 2003; 1634:1–14. [PubMed: 14563408]

86. Harper NJ, Sathasivam N, Delikatny EJ. The mitochondrial permeability transition inhibitor, cyclosporin A, induces NMR-visible lipid via a chlorpromazine dependent pathway. Proc Int Soc Mag Reson Med. 2000; 8

87. Sathasivam N, Delikatny EJ. Time-dependent inhibition of 5-fluorouracil-induced NMR-visible lipid accumulation. Proc Int Soc Magn Reson Med. 2002; 10:2142.

88. Leung DJ, Mawn TM, Delikatny EJ. Comparison of MRS with fluorescence for molecular imaging and determination of phospholipase isoforms. Proc Intl Soc Magn Reson Med. 2009; 17:200.

89. Liimatainen TJ, Erkkila AT, Valonen P, Vidgren H, Lakso M, Wong G, Grohn OH, Yla-Herttuala S, Hakumaki JM. 1H MR spectroscopic imaging of phospholipase-mediated membrane lipid release in apoptotic rat glioma in vivo. Magn Reson Med. 2008; 59:1232–1238. [PubMed: 18506792]

90. Haase A, Frahm J, Matthaei D, Hanicke W, Bomsdorf H, Kunz D, Tischler R. MR imaging using stimulated echoes (STEAM). Radiology. 1986; 160:787–790. [PubMed: 3737918]

91. Bottomley PA. Spatial localization in NMR spectroscopy in vivo. Ann N Y Acad Sci. 1987; 508:333–348. [PubMed: 3326459]

92. Ordidge, RJ.; Bendall, MR.; Gordon, RE.; Connelly, A. Volume selection for in vivo biological spectroscopy. In: Govil, G.; Khetrapal, CL.; Saran, A., editors. Magnetic resonance in biology and medicine. McGraw Hill; New Delhi, India: 1985. p. 387-397.

93. Shungu DC, Glickson JD. Band-selective spin echoes for in vivo localized 1H NMR spectroscopy. Magn Reson Med. 1994; 32:277–284. [PubMed: 7984059]

94. Remy C, Arus C, Ziegler A, Lai ES, Moreno A, Le Fur Y, Decorps M. In vivo, ex vivo, and in vitro one- and two-dimensional nuclear magnetic resonance spectroscopy of an intracerebral glioma in rat brain: assignment of resonances. J Neurochem. 1994; 62:166–179. [PubMed: 8263516]

95. Schmitz JE, Kettunen MI, Hu DE, Brindle KM. 1H MRS-visible lipids accumulate during apoptosis of lymphoma cells in vitro and in vivo. Magn Reson Med. 2005; 54:43–50. [PubMed: 15968678]

96. He Q, Shungu DC, van Zijl PC, Bhujwalla ZM, Glickson JD. Single-scan in vivo lactate editing with complete lipid and water suppression by selective multiple-quantum-coherence transfer (Sel-MQC) with application to tumors. Journal of Magnetic Resonance Series B. 1995; 106:203–211. [PubMed: 7719620]

97. Lee SC, Huang MQ, Nelson DS, Pickup S, Wehrli S, Adegbola O, Poptani H, Delikatny EJ, Glickson JD. In vivo MRS markers of response to CHOP chemotherapy in the WSU-DLCL2 human diffuse large B-cell lymphoma xenograft. NMR Biomed. 2008; 21:723–733. [PubMed: 18384181]

98. Mellon EA, Lee SC, Pickup S, Kim S, Goldstein SC, Floyd TF, Poptani H, Delikatny EJ, Reddy R, Glickson JD. Detection of lactate with a hadamard slice selected, selective multiple quantum coherence, chemical shift imaging sequence (HDMD-SelMQC-CSI) on a clinical MRI scanner: Application to tumors and muscle ischemia. Magn Reson Med. 2009; 62:1404–1413. [PubMed: 19785016]

99. Sotak CH. Multiple quantum NMR spectroscopy methods for measuring the apparent self-diffusion coefficient of in vivo lactic acid. NMR Biomed. 1991; 4:70–72. [PubMed: 1859787]

100. Nicolay K, Braun KP, Graaf RA, Dijkhuizen RM, Kruiskamp MJ. Diffusion NMR spectroscopy. NMR Biomed. 2001; 14:94–111. [PubMed: 11320536]

101. Liu Y. Fatty acid oxidation is a dominant bioenergetic pathway in prostate cancer. Prostate Cancer Prostatic Dis. 2006; 9:230–234. [PubMed: 16683009]

102. Wang F, Kumagai-Braesch M, Herrington MK, Larsson J, Permert J. Increased lipid metabolism and cell turnover of MiaPaCa2 cells induced by high-fat diet in an orthotopic system. Metabolism. 2009; 58:1131–1136. [PubMed: 19493551]

103. Ross BD, Chenevert TL, Kim B, Ben-Yoseph O. Magnetic resonance imaging and spectroscopy: application to experimental neuro-oncology. Quart Magn Reson Biol and Medicine. 1994; 1:89–106.

104. Liimatainen T, Hakumaki J, Tkac I, Grohn O. Ultra-short echo time spectroscopic imaging in rats: implications for monitoring lipids in glioma gene therapy. NMR Biomed. 2006; 19:554–559. [PubMed: 16523527]

105. Griffin JL, Lehtimaki KK, Valonen PK, Grohn OHJ, Kettunen MI, Yla-Herttuala S, Pitkanen A, Nicholson JK, Kauppinen RA. Assignment of 1H Nuclear Magnetic Resonance Visible Polyunsaturated Fatty Acids in BT4C Gliomas Undergoing Ganciclovir-Thymidine Kinase Gene Therapy-induced Programmed Cell Death. Cancer Res. 2003; 63:3195–3201. [PubMed: 12810648]

106. Liimatainen T, Hakumaki JM, Kauppinen RA, Ala-Korpela M. Monitoring of gliomas in vivo by diffusion MRI and (1)H MRS during gene therapy-induced apoptosis: interrelationships between water diffusion and mobile lipids. NMR Biomed. 2009; 22:272–279. [PubMed: 19009568]

107. Liimatainen T, Lehtimaki K, Ala-Korpela M, Hakumaki J. Identification of mobile cholesterol compounds in experimental gliomas by (1)H MRS in vivo: effects of ganciclovir-induced apoptosis on lipids. FEBS Lett. 2006; 580:4746–4750. [PubMed: 16893542]

108. Mountford CE, Delikatny EJ, Dyne M, Holmes KT, Mackinnon WB, Ford R, Hunter JC, Truskett ID, Russell P. Uterine punch biopsy specimens can be analyzed by ^{1}H MRS. Magn Reson Med. 1990; 13:324–331. [PubMed: 2314221]

109. Mackinnon WB, Russell P, May GL, Mountford CE. Characterisation of human ovarian epithelial tumours (*ex vivo*) by proton magnetic resonance spectroscopy. Int J Gynaecol Oncology. 1995; 5:211–221.

110. Hahn P, Smith IC, Leboldus L, Littman C, Somorjai RL, Bezabeh T. The classification of benign and malignant human prostate tissue by multivariate analysis of 1H magnetic resonance spectra. Canc Res. 1997; 57:3398–3401.

111. Swindle P, McCredie S, Russell P, Himmelreich U, Khadra M, Lean C, Mountford C. Pathologic characterization of human prostate tissue with proton MR spectroscopy. Radiology. 2003; 228:144–151. [PubMed: 12832578]

112. Mackinnon WB, Huschtscha L, Dent K, Hancock R, Paraskeva C, Mountford CE. Correlation of cellular differentiation in human colorectal carcinoma and adenoma cell lines with metabolite profiles determined by ^{1}H magnetic resonance spectroscopy. Int J Cancer. 1994; 59:248–261. [PubMed: 7927926]

113. Russell P, Lean CL, Delbridge L, May GL, Dowd S, Mountford CE. Proton magnetic resonance and human thyroid neoplasia I: discrimination between benign and malignant neoplasms. Am J Med. 1994; 96:383–388. [PubMed: 8166160]

114. Lean CL, Newland RC, Ende DA, Bokey EL, Smith ICP, Mountford CE. Assessment of human colorectal biopsies by ^{1}H MRS: correlation with histopathology. Magn Reson Med. 1993; 30:525–533. [PubMed: 8259052]

115. Moreno A, Rey M, Montane J, Alonso J, Arus C. ^{1}H NMR spectroscopy of colon tumors and normal mucosal biopsies; elevated taurine levels and reduced polyethyleneglycol absorption in tumors may have diagnostic significance. NMR Biomed. 1993; 6:111–118. [PubMed: 8388705]

116. Mackinnon WB, Barry PA, Malycha PL, Gillett DJ, Russell P, Lean CL, Doran ST, Barraclough BH, Bilous M, Mountford CE. Fine-needle biopsy specimens of benign breast lesions distinguished from invasive cancer ex vivo with proton MR spectroscopy. Radiology. 1997; 204:661–666. [PubMed: 9280241]

117. Ende D, Rutter A, Russell P, Mountford CE. Chemical shift imaging of human colorectal tissue (*ex vivo*). NMR Biomed. 1996; 9:179–183. [PubMed: 9015805]

118. Briere KM, Kuesel AC, Bird RP, Smith IC. 1H MR visible lipids in colon tissue from normal and carcinogen-treated rats. NMR Biomed. 1995; 8:33–40. [PubMed: 7547183]

119. Kuesel AC, Briere KM, Halliday WC, Sutherland GR, Donnelly SM, Smith IC. Mobile lipid accumulation in necrotic tissue of high grade astrocytomas. Anticancer Res. 1996; 16:1485–1489. [PubMed: 8694517]

120. deSouza NM, Soutter WP, Rustin G, Mahon MM, Jones B, Dina R, McIndoe GA. Use of neoadjuvant chemotherapy prior to radical hysterectomy in cervical cancer: monitoring tumour shrinkage and molecular profile on magnetic resonance and assessment of 3-year outcome. Br J Cancer. 2004; 90:2326–2331. [PubMed: 15162152]

121. Mahon MM, Cox IJ, Dina R, Soutter WP, McIndoe GA, Williams AD, deSouza NM. (1)H magnetic resonance spectroscopy of preinvasive and invasive cervical cancer: in vivo-ex vivo profiles and effect of tumor load. J Magn Reson Imaging. 2004; 19:356–364. [PubMed: 14994305]

122. Mahon MM, deSouza NM, Dina R, Soutter WP, McIndoe GA, Williams AD, Cox IJ. Preinvasive and invasive cervical cancer: an ex vivo proton magic angle spinning magnetic resonance spectroscopy study. NMR Biomed. 2004; 17:144–153. [PubMed: 15137039]

123. Mahon MM, Williams AD, Soutter WP, Cox IJ, McIndoe GA, Coutts GA, Dina R, deSouza NM. 1H magnetic resonance spectroscopy of invasive cervical cancer: an in vivo study with ex vivo corroboration. NMR Biomed. 2004; 17:1–9. [PubMed: 15011245]

124. Lyng H, Sitter B, Bathen TF, Jensen LR, Sundfor K, Kristensen GB, Gribbestad IS. Metabolic mapping by use of high-resolution magic angle spinning 1H MR spectroscopy for assessment of apoptosis in cervical carcinomas. BMC Cancer. 2007; 7:11. [PubMed: 17233882]

125. Zietkowski D, Davidson RL, Eykyn TR, De Silva SS, Desouza NM, Payne GS. Detection of cancer in cervical tissue biopsies using mobile lipid resonances measured with diffusion-weighted (1)H magnetic resonance spectroscopy. NMR Biomed. 2009

126. Stenman K, Hauksson JB, Grobner G, Stattin P, Bergh A, Riklund K. Detection of polyunsaturated omega-6 fatty acid in human malignant prostate tissue by 1D and 2D high-resolution magic angle spinning NMR spectroscopy. MAGMA. 2009; 22:327–331. [PubMed: 19921294]

127. Opstad KS, Bell BA, Griffiths JR, Howe FA. An investigation of human brain tumour lipids by high-resolution magic angle spinning 1H MRS and histological analysis. NMR Biomed. 2008; 21:677–685. [PubMed: 18186027]

128. Opstad KS, Wright AJ, Bell BA, Griffiths JR, Howe FA. Correlations between in vivo (1)H MRS and ex vivo (1)H HRMAS metabolite measurements in adult human gliomas. J Magn Reson Imaging. 2010; 31:289–297. [PubMed: 20099340]

129. Poptani H, Gupta RK, Roy R, Pandey R, Jain VK, Chhabra DK. Characterization of intracranial mass lesions with in vivo proton MR spectroscopy. AJNR Am J Neuroradiol. 1995; 16:1593–1603. [PubMed: 7502961]

130. Poptani H, Gupta RK, Jain VK, Roy R, Pandey R. Cystic intracranial mass lesions: possible role of in vivo MR spectroscopy in its differential diagnosis. Magn Reson Imaging. 1995; 13:1019–1029. [PubMed: 8583866]

131. Opstad KS, Ladroue C, Bell BA, Griffiths JR, Howe FA. Linear discriminant analysis of brain tumour (1)H MR spectra: a comparison of classification using whole spectra versus metabolite quantification. NMR Biomed. 2007; 20:763–770. [PubMed: 17326043]

132. Wright AJ, Fellows G, Byrnes TJ, Opstad KS, McIntyre DJ, Griffiths JR, Bell BA, Clark CA, Barrick TR, Howe FA. Pattern recognition of MRSI data shows regions of glioma growth that agree with DTI markers of brain tumor infiltration. Magn Reson Med. 2009; 62:1646–1651. [PubMed: 19785020]

133. Calvar JA, Meli FJ, Romero C, Calcagno ML, Yanez P, Martinez AR, Lambre H, Taratuto AL, Sevlever G. Characterization of brain tumors by MRS, DWI and Ki-67 labeling index. J Neurooncol. 2005; 72:273–280. [PubMed: 15937653]

134. Majos C, Alonso J, Aguilera C, Serrallonga M, Perez-Martin J, Acebes JJ, Arus C, Gili J. Proton magnetic resonance spectroscopy ((1)H MRS) of human brain tumours: assessment of differences between tumour types and its applicability in brain tumour categorization. Eur Radiol. 2003; 13:582–591. [PubMed: 12594562]

135. Negendank WG. MR spectroscopy of musculoskeletal soft-tissue tumors [Review]. Magn Reson Imaging Clin N Am. 1995; 3:713–725. [PubMed: 8564691]

136. Opstad KS, Murphy MM, Wilkins PR, Bell BA, Griffiths JR, Howe FA. Differentiation of metastases from high-grade gliomas using short echo time 1H spectroscopy. J Magn Reson Imaging. 2004; 20:187–192. [PubMed: 15269942]

137. Chawla S, Yang Z, S W, S C, C C, DM OR, A V, ER M, H P. Proton MR spectroscopy in differentiating glioblastomas from primary cerebral lymphomas and brain metastases. J Comp Assist Tomography. in press.

138. Sjobakk TE, Johansen R, Bathen TF, Sonnewald U, Kvistad KA, Lundgren S, Gribbestad IS. Metabolic profiling of human brain metastases using in vivo proton MR spectroscopy at 3T. BMC Cancer. 2007; 7:141. [PubMed: 17662122]

139. Chernov MF, Hayashi M, Izawa M, Usukura M, Yoshida S, Ono Y, Muragaki Y, Kubo O, Hori T, Takakura K. Multivoxel proton MRS for differentiation of radiation-induced necrosis and tumor recurrence after gamma knife radiosurgery for brain metastases. Brain Tumor Pathol. 2006; 23:19–27. [PubMed: 18095115]

140. Koeller KK, Smirniotopoulos JG, Jones RV. Primary central nervous system lymphoma: radiologic-pathologic correlation. Radiographics. 1997; 17:1497–1526. [PubMed: 9397461]

141. Harting I, Hartmann M, Jost G, Sommer C, Ahmadi R, Heiland S, Sartor K. Differentiating primary central nervous system lymphoma from glioma in humans using localised proton magnetic resonance spectroscopy. Neurosci Lett. 2003; 342:163–166. [PubMed: 12757890]

142. Ducreux D, Wu RH, Mikulis DJ, terBrugge K. Diffusion-weighted imaging and single-voxel MR spectroscopy in a case of malignant cerebral lymphoma. Neuroradiology. 2003; 45:865–868. [PubMed: 14605786]

143. Jayasundar R, Raghunathan P, Banerji AK. Proton MRS similarity between central nervous system non-Hodgkin lymphoma and intracranial tuberculoma. Magn Reson Imaging. 1995; 13:489–493. [PubMed: 7791559]

144. Burtscher IM, Skagerberg G, Geijer B, Englund E, Stahlberg F, Holtas S. Proton MR spectroscopy and preoperative diagnostic accuracy: an evaluation of intracranial mass lesions

characterized by stereotactic biopsy findings. AJNR Am J Neuroradiol. 2000; 21:84–93. [PubMed: 10669230]

145. Kizu O, Naruse S, Furuya S, Morishita H, Ide M, Maeda T, Ueda S. Application of proton chemical shift imaging in monitoring of gamma knife radiosurgery on brain tumors. Magn Reson Imaging. 1998; 16:197–204. [PubMed: 9508276]

146. Rock JP, Hearshen D, Scarpace L, Croteau D, Gutierrez J, Fisher JL, Rosenblum ML, Mikkelsen T. Correlations between magnetic resonance spectroscopy and image-guided histopathology, with special attention to radiation necrosis. Neurosurgery. 2002; 51:912–919. discussion 919-920. [PubMed: 12234397]

147. Kimura T, Sako K, Tanaka K, Gotoh T, Yoshida H, Aburano T, Tanaka T, Arai H, Nakada T. Evaluation of the response of metastatic brain tumors to stereotactic radiosurgery by proton magnetic resonance spectroscopy, 201TlCl single-photon emission computerized tomography, and gadolinium-enhanced magnetic resonance imaging. J Neurosurg. 2004; 100:835–841. [PubMed: 15137602]

148. Asao C, Korogi Y, Kitajima M, Hirai T, Baba Y, Makino K, Kochi M, Morishita S, Yamashita Y. Diffusion-weighted imaging of radiation-induced brain injury for differentiation from tumor recurrence. AJNR Am J Neuroradiol. 2005; 26:1455–1460. [PubMed: 15956515]

149. Knopp EA, S Cha, Johnson G, Mazumdar A, Golfinos JG, Zagzag D, Miller DC, Kelly PJ, Kricheff II. Glial neoplasms: dynamic contrast-enhanced T2*-weighted MR imaging. Radiology. 1999; 211:791–798. [PubMed: 10352608]

150. Hein PA, Eskey CJ, Dunn JF, Hug EB. Diffusion-weighted imaging in the follow-up of treated high-grade gliomas: tumor recurrence versus radiation injury. AJNR Am J Neuroradiol. 2004; 25:201–209. [PubMed: 14970018]

151. Hansen SH, Andersen ML, Cornett C, Gradinaru R, Grunnet N. A role for taurine in mitochondrial function. J Biomed Sci. 2010; 17(1):S23. [PubMed: 20804598]

152. Rosi A, Luciani AM, Matarrese P, Arancia G, Viti V, Guidoni L. ^{1}H-MRS lipid signal modulation and morphological and ultrastructural changes related to tumor cell proliferation. Magn Reson Med. 1999; 42:248–257. [PubMed: 10440949]

153. Rosi A, Grande S, Luciani AM, Barone P, Mlynarik V, Viti V, Guidoni L. (1H) MRS studies of signals from mobile lipids and from lipid metabolites: comparison of the behavior in cultured tumor cells and in spheroids. NMR Biomed. 2004; 17:76–91. [PubMed: 15052555]

154. Callies R, Sri-Pathmanathan RM, Ferguson DY, Brindle KM. The appearance of neutral lipid signals in the 1H NMR spectra of a myeloma cell line correlates with the induced formation of cytoplasmic lipid droplets. Magn Reson Med. 1993; 29:546–550. [PubMed: 8464371]

155. Kotitschke K, Jung H, Nekolla S, Haase A, Bauer A, Bogdahn U. High-resolution one- and two-dimensional 1H-MRS of human brain tumor and normal glial cells. NMR Biomed. 1994; 7:111–120. [PubMed: 8080712]

156. Chen JH, Enloe BM, Weybright P, Campbell N, Dorfman D, Fletcher CD, Cory DG, Singer S. Biochemical correlates of thiazolidinedione-induced adipocyte differentiation by high-resolution magic angle spinning NMR spectroscopy. Magn Reson Med. 2002; 48:602–610. [PubMed: 12353276]

157. Wright LC, Djordjevic JT, Schibeci SD, Himmelreich U, Muljadi N, Williamson P, Lynch GW. Detergent-resistant membrane fractions contribute to the total 1H NMR-visible lipid signal in cells. Eur J Biochem. 2003; 270:2091–2100. [PubMed: 12709069]

158. May GL, Wright LC, Groot Obbink K, Byleveld P, Garg M, Ahmad Z, Sorrell TC. Increased saturated triacylglycerol levels in plasma membranes of human neutrophils stimulated by lipopolysaccharide. J Lipid Res. 1997; 38:1562–1570. [PubMed: 9300778]

159. May GL, Sztelma K, Sorrell TC, Mountford CE. Comparison of human polymorphonuclear leukocytes from peripheral blood and purulent exudates by high-resolution ^{1}H MRS. Magn Reson Med. 1991; 19:191–198. [PubMed: 2046533]

160. Santini MT, Romano R, Rainaldi G, Indovina P, Ferrante A, Motta A, Indovina PL. Temporal dynamics of 1H-NMR-visible metabolites during radiation-induced apoptosis in MG-63 human osteosarcoma spheroids. Radiat Res. 2006; 166:734–745. [PubMed: 17067211]

161. Santini MT, Romano R, Rainaldi G, Ferrante A, Motta A, Indovina PL. Increases in 1H-NMR mobile lipids are not always associated with overt apoptosis: evidence from MG-63 human osteosarcoma three-dimensional spheroids exposed to a low dose (2 Gy) of ionizing radiation. Radiat Res. 2006; 165:131–141. [PubMed: 16435912]

162. Luciani AM, Rosi A, Maggiorella MT, Federico M, Sulli N, Verani P, Rossi GB, Viti V, Guidoni L. Interaction of HIV-1 with susceptible lymphoblastoid cells. 1H NMR studies. FEBS Lett. 1991; 285:11–16. [PubMed: 1712316]

163. Ferretti A, Knijn A, Raggi C, Sargiacomo M. High-resolution proton NMR measures mobile lipids associated with Triton-resistant membrane domains in haematopoietic K562 cells lacking or expressing caveolin-1. European Journal of Biophysics. 2002; 32:83–95.

164. Le Moyec L, Tatoud R, Degeorges A, Calabresse C, Bauza G, Eugène M, Calvo F. Proton nuclear magnetic resonance spectroscopy reveals cellular lipids involved in resistance to adriamycin and taxol by the K562 leukaemia cell line. Cancer Res. 1996; 56:3461–3467. [PubMed: 8758912]

165. Santini MT, Romano R, Rainaldi G, Filippini P, Bravo E, Porcu L, Motta A, Calcabrini A, Meschini S, Indovina PL, Arancia G. The relationship between 1H-NMR mobile lipid intensity and cholesterol in two human tumor multidrug resistant cell lines (MCF-7 and LoVo). Biochim Biophys Acta. 2001; 1531:111–131. [PubMed: 11278177]

Abbreviations

CoA	coenzyme A
Cho	choline
COSY	Correlated Spectroscopy
cPLA2	cytosolic phospholipase A2
Cr/PCr	creatine/phosphocreatine
GPC	*sn*-glycero-3-phosphocholine
HMG-CoA	hydroxymethylglutaryl-coenzyme A
HSV-*tk*	herpes simplex virus thymidine kinase
iPLA2	calcium independent phospholipase A2
IFN	interferon
MRI	magnetic resonance imaging
MRS	magnetic resonance spectroscopy
NAA	N-acetylaspartate
NTP	nucleoside triphosphate
PB	phenylbutyrate
PC	phosphocholine
PCLs	Primary cerebral lymphomas
PLA1,PLA2	phospholipase A1, phospholipase A2
PPAR	peroxisome proliferator-activated receptor
PRESS	Point Resolved Spectroscopy
PUFA	polyunsaturated fatty acids
STEAM	Stimulated Echo Acquisition Mode

T_2	spin-spin or transverse relaxation time
tCho	total choline
TPP	tetraphenylphosphonium chloride
TUNEL	terminal deoxynucleotidyl transferase dUTP nick end labeling
WHO	World Health Organization
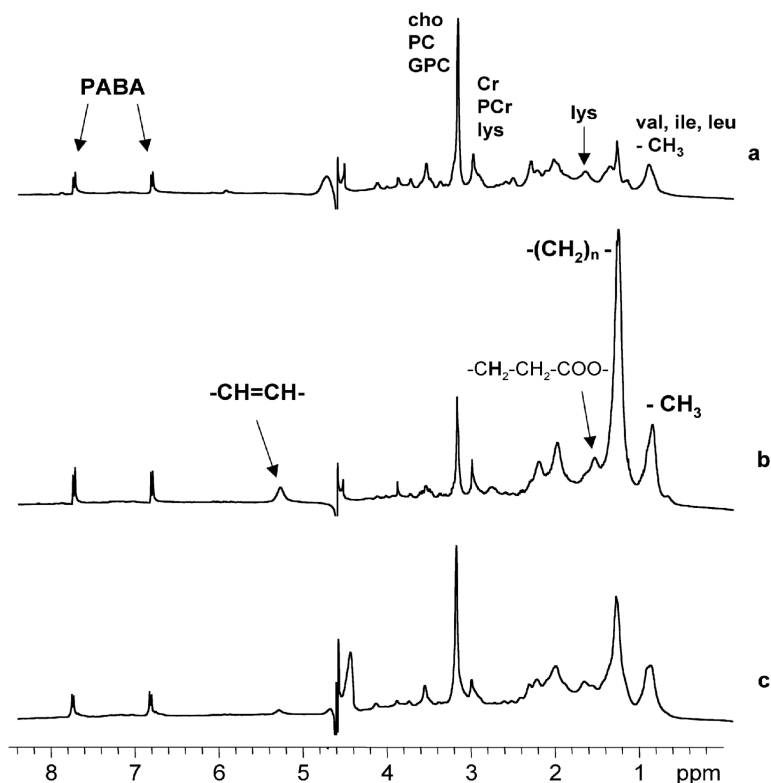
**Figure 1.**
One-dimensional 1H MR spectra of HBL-100 transformed human breast cells treated with (a) PBS (control cells), (b) 6.25 µM TPP, (c) 6.25 µM TPP and 25 µM chlorpromazine for 48 h. Spectrum (a) from control cells shows resonances only from mobile amino acids (the mobile proteome) and small molecular weight metabolites. Spectrum (b) from cells treated with the mitochondrial toxin TPP is dominated by resonances from MR-visible or mobile lipids at 0.9, 1.3, 1.6, 2.0, 2.8 and 5.3 ppm. Spectrum (c) shows that pretreatment with the lysomotropic agent chlorpromazine substantially reduced mobile lipid resonances indicating lysosomal involvement in drug-induced lipid accumulations. Abbreviations: cho: choline, PC: phosphocholine, GPC: glycerophosphocholine, Cr: creatine, PCr: phosphocreatine, lys: lysine, val: valine, ile: isoleucine, leu: leucine, PABA: para-aminobenzoic acid, a chemical shift and concentration reference that was added in an internal capillary. Adapted from [2] and reprinted with permission.
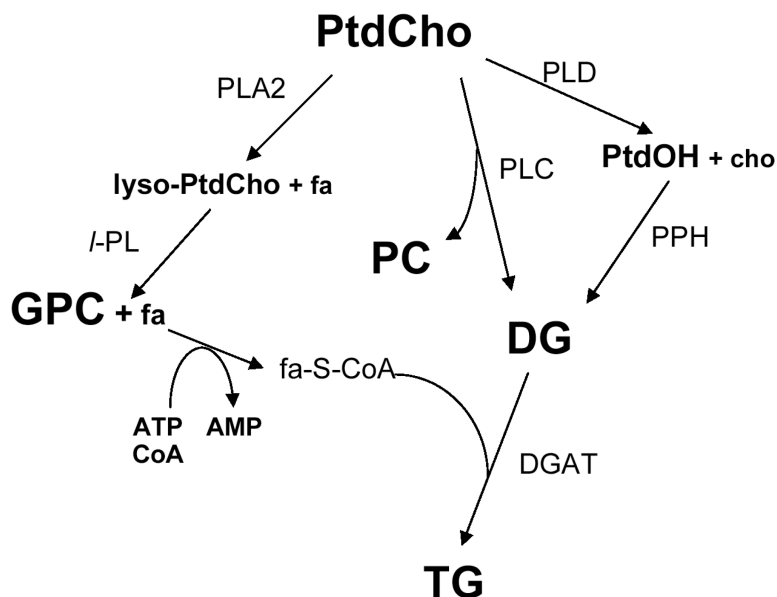
Figure 2.
Metabolic flow chart showing the phosphatidylcholine cycle of phospholipid metabolism
and the pathways leading to the production of triglycerides. The final step in triglyceride
synthesis occurs in the endoplasmic reticulum and is the condensation of an activated fatty
acid (fa-S-CoA) with diacylglycerol (DG) via the enzyme diacylglycerolacyltransferase
(DGAT). The flow chart shows other key pathways in phosphatidylcholine catabolism. Most
notably, during cell stress the catabolic production of GPC arises from the consecutive
removal of fatty acyl chains from phosphatidylcholine by phospholipase A2 and
lysosphospholipase. The fatty acids released can be reesterified into phospholipids or
converted into triglycerides. *Enzymes:* **DGAT**, diacylglycerolacyltransferase (E.C.
2.3.1.20); **GPC-PDE**, GPC-phosphodiesterase (E.C. 3.1.4.2); **PLA2**, phospholipase A2
(E.C. 3.1.1.4); ***l*-PL**, lysophospholipase (E.C. 3.1.1.5); **PLC**, phospholipase C (E.C. 3.1.4.3);
PLD, phospholipase D (E.C. 3.1.4.4); **PPH**, phosphatidate phosphohydrolase (E.C. 3.1.3.4).
Metabolites: **cho**, choline; **DG**, 1,2-diacylglycerol; **PtdOH**, phosphatidic acid, **PC**,
phosphocholine, **PtdCho**, phosphatidylcholine; **TG**, triacylglycerol (triglycerides). Adapted
from [46] and reprinted with permission.
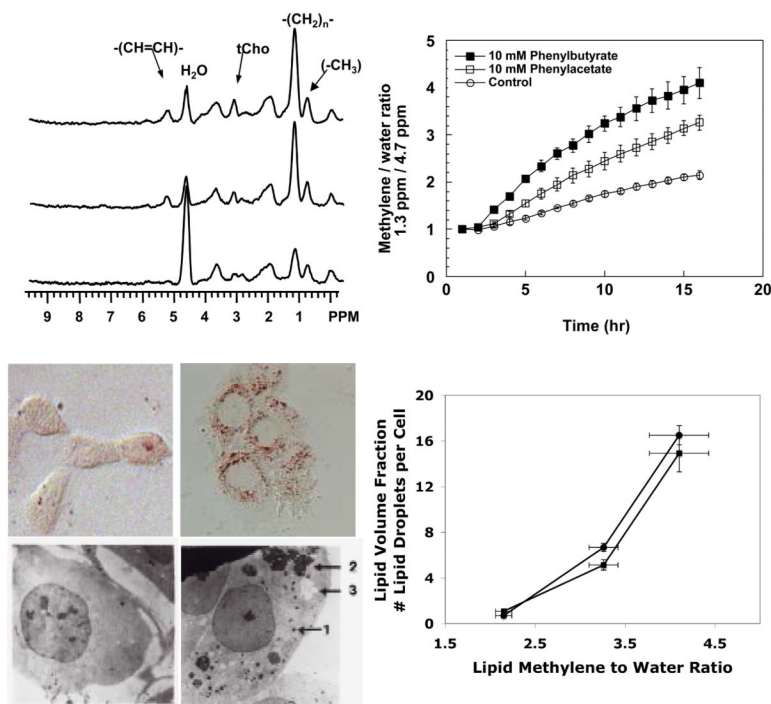
Figure 3.
Induction of MR-visible lipids by differentiating agents in prostate cancer cells. The upper left panel shows ^{1}H MR spectra of DU145 cells grown on Biosilon beads and perfused in the magnet. From the top, the three traces are: treated with 10 mM PB for 16 h, treated with 10 mM phenylacetate for 16 h, control. The top right panel shows the relative increase of the methylene to water ratio (1.3 ppm / 4.7 ppm). The relative increase in MR-visible lipid is greater when cells are treated with PB compared to phenylacetate or control. The bottom left panel shows oil red O and electron micrographs of control cells (left) and cells treated with PB (right), demonstrating the increase in cytoplasmic lipid droplets that accompany drug treatment. The bottom right panel plots number of lipid droplets per cell (circles) and the cellular volume fraction occupied by lipid droplets (squares) as a function of the methylene to water ratio showing a linear relationship for both measures for control, phenylacetate and PB-treated cells. Adapted from [46] and [45] and reprinted with permission.
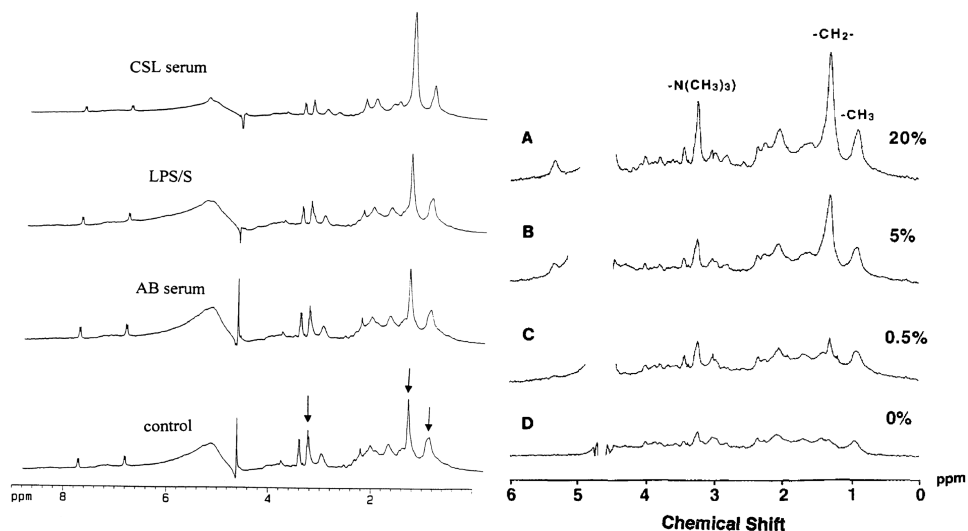
Figure 4.
MR-visible lipid spectra can be modulated by external serum levels. On the left, ^{1}H MR 1D spectra obtained from neutrophils incubated in Hanks' balanced salt solution (control), AB serum containing low levels of fatty acids, lipopolysaccharide (LPS), and CSL serum containing high levels of fatty acids. The levels of lipid accumulation are higher in the CSL serum than in cells stimulated with LPS. The arrows indicate the lipid methylene peak at 1.3 ppm, the methyl peak at 0.9 ppm, and the taurine/choline peak at 3.2 ppm. The internal standard, p-aminobenzoic acid produces two doublets, one at 6.83 and the other at 7.83 ppm. On the right hand side, the level of mobile lipids in human mixed peripheral blood lymphocyte cultures is directly dependent on the amount of human serum in the culture medium. Note in both sets of spectra the presence of resonances at 3.2 and 3.4 ppm indicating high levels of taurine as well as choline. Taurine is present in the cytoplasm of immune cells at high concentrations where it acts as an osmolyte and radioprotectant.
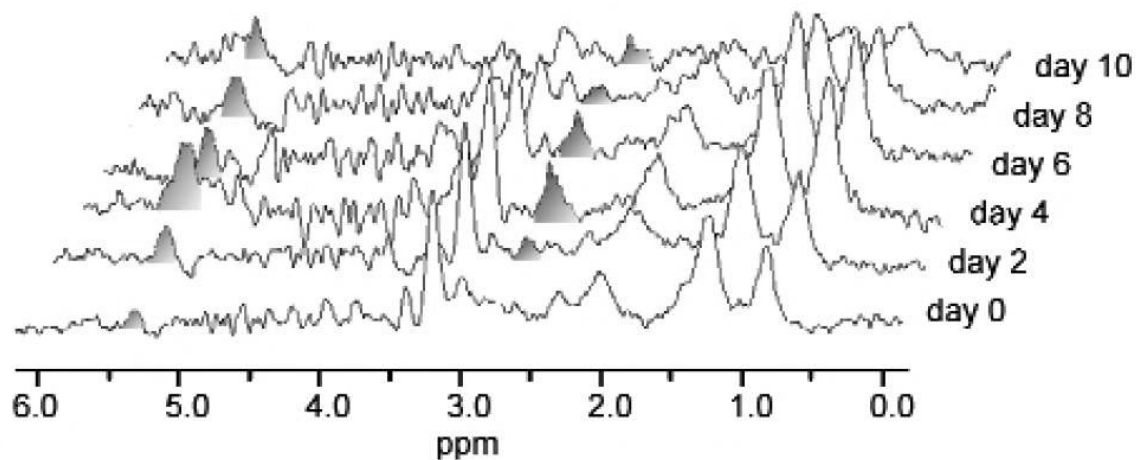
Figure 5.
Sequential single voxel MR spectra from an HSV-*tk* positive rat BT4C glioma. The spectrum from the tumor before treatment (day 0), shows strong resonances from the mobile lipid methylene resonance at 1.3 ppm and tCho at 3.2 ppm. Treatment with ganciclovir leads to increases in the PUFA resonances (shaded peaks) at 2.8 and 5.3 ppm, as well as in the mobile lipid resonances at 0.9 and 1.3 ppm. These increases were highest at 4 days, which correlated with maximum apoptosis. A decrease in all metabolite resonances was seen after 8 days of treatment, which correlated with formation of scar tissue in the tumor. Reprinted with permission from [50].
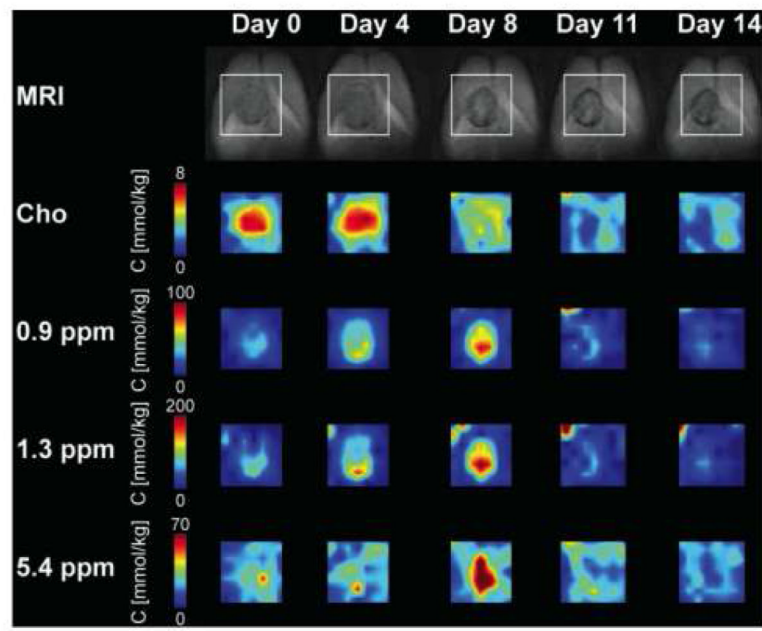
Figure 6.
MR images of a rat brain containing an HSV-*tk* positive BT4C glioma undergoing ganciclovir treatment. The top row shows T_2-weighted coronal plane images with the region of interest for the CSI studies (box). The spatial change in tCho, mobile lipids (0.9 and 1.3 ppm) and PUFA (5.3 ppm) after treatment is shown by the CSI maps. An increase in mobile lipid concentration was observed for 8 days followed by reduction to baseline levels. This correlated with a decrease in tCho levels. Reprinted with permission from [89].
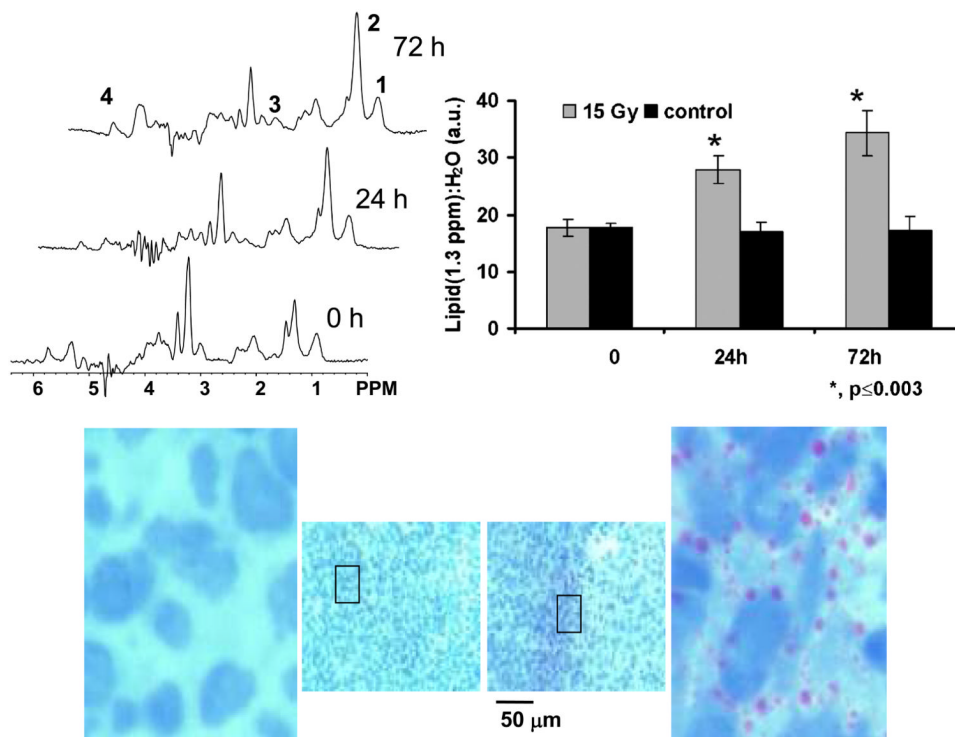
Figure 7.
Representative MR spectra and histological sections from a subcutaneously implanted human diffuse large B cell lymphoma xenograft showing changes in ML resonances after radiation therapy. (a) The top left panel shows spectra from a tumor before treatment and at 24 h and 72 h after 15 Gy irradiation. Labeled resonances are from: 1: lipid methyl (CH_3 at 0.9 ppm); 2: methylene ($(-CH_2-)_n$ at 1.3 ppm); 3: polyunsaturated fatty acid (-CH=CH-CH_2-CH=CH- at 2.8 ppm) and 4: unsaturated fatty acids (-CH=CH- at 5.3 ppm). The ratio of the mobile lipid resonance at 1.3 ppm to unsuppressed water area (upper right panel) shows a significant increase in mobile lipids in treated tumors (grey bars) in comparison to untreated control tumors (black bars). The histological sections stained with hematoxylin and oil red O in the bottom panel shows the increase in perinuclear lipid droplets (red) after 72 h treatment (right) compared to controls (left). Adapted from [49] and reprinted with permission.
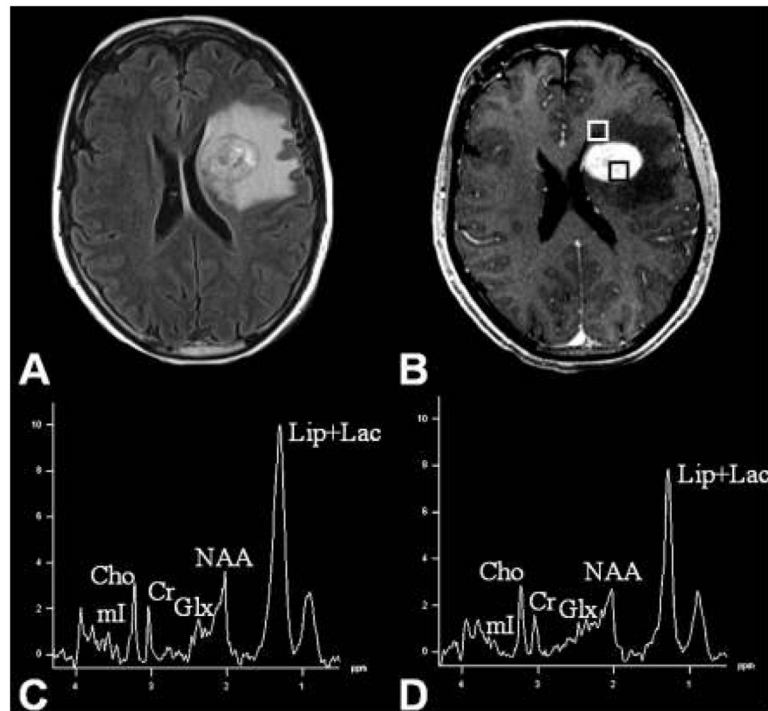
Figure 8.
Fluid attenuated inversion recovery (FLAIR, A) and post contrast enhanced T_1-weighted MRI image (B) from a patient with primary cerebral diffuse large B cell lymphoma (PCL). Boxes in (B) show voxels from contrast-enhancing and peritumoral regions. The MR spectra from the contrast enhanced area (C) as well as the peritumoral region (D) show elevated choline and mobile lipid resonances indicating the infiltrative nature of the neoplasm. The mobile lipid resonances are probably due to the presence of infiltrative lymphocytes. Reprinted with permission from [137].

Table 1
Observed Resonances in 1D proton MR spectra of cells and tissues

Chemical Shift (ppm)	Molecule	Species (bold face)
Lipid		
0.89	fatty acyl chain	**CH**$_3$-CH$_2$-CH$_2$-
1.28	fatty acyl chain	-CH$_2$-**CH**$_2$-CH$_2$-
1.58	fatty acyl chain	-**CH**$_2$-CH$_2$-COO$^-$
2.03	fatty acyl chain	-CH=CH-**CH**$_2$-
2.24	fatty acyl chain	-CH$_2$-**CH**$_2$-COO$^-$
2.88	fatty acyl chain	-CH=CH-**CH**$_2$-CH=CH-
4.30	glycerol backbone	R1-O-**CH**$_2$-CH(O-R2)-**CH**$_2$(O-R3)
5.32	fatty acyl chain	-**CH=CH**-
Amino Acids		
0.9-1.0	aliphatic branched chain amino acids (val, leu, ile)	**CH**$_3$-
1.33	threonine	**CH**$_3$-CH-
1.49	alanine	**CH**$_3$-CH-
1.71	lysine/polyamines	H$_3$N$^+$-CH$_2$-**CH**$_2$-CH$_2$-
2.03	N-acetylaspartate	**CH**$_3$-COO$^-$NH
2.17	glutamate/glutamine	CH-**CH**$_2$-CH$_2$-COO$^-$/-NH$_3^+$
3.02	lysine	H$_3$N$^+$-**CH**$_2$-CH$_2$-CH$_2$-
3.78	alanine/glu/gln and other amino acids	α - protons –OOC-**CH**(R)-NH-
Small Molecular Weight Metabolites		
1.33	lactate	**CH**$_3$-CH-
3.02	creatine	**CH**$_3$-N-CH$_2$-COO$^-$
3.02	phosphocreatine	**CH**$_3$-N-CH$_2$-COO$^-$
3.21	choline	-N$^+$(**CH**$_3$)$_3$
3.23	phosphocholine	-N$^+$(**CH**$_3$)$_3$
3.24	glycerophosphocholine	-N$^+$(**CH**$_3$)$_3$
3.25	*myo*-inositol	-CH-**CH**(OH)-
3.25	taurine	H$_3$N$^+$-**CH**$_2$-CH$_2$-SO$_3$-
3.43	taurine	H$_3$N$^+$-CH$_2$-**CH**$_2$-SO$_3$-
4.63	water	**H**$_2$O, **H**OD

This table lists contributors to the major resonances observed in 1D spectra of cells and tissues. The protons giving rise to each resonance are highlighted in bold. Taurine assignments are taken from [151]. Many resonances are composite and consist of varying contributions of many species. This list is not to be considered exhaustive. (adapted from [1]).

Table 2

Effectors and Inhibitors of Inducible Mobile Lipid in Cell Models

Mobile Lipid Effector	Cell/Tissue Type	Mobile Lipid Inhibitor	Reference
Culture Conditions			
Low pH	Transformed murine L fibroblasts C6 glioma cells	Reversible at neutral pH	[16][44, 68]
High cell density	Transformed murine L fibroblasts C6 glioma cells		[16][41, 42, 44, 68]
Cell subculture	HeLa cells	Time in culture	[152]
	MCF-7 cells		[153]
Grown in culture	Human peripheral blood monocytes		[24]
Serum deprivation	Transformed murine L fibroblasts		[16]
	Jurkat T lymphoblasts		[72]
Serum	Mixed peripheral blood cells		[24]
	Human neutrophils		[21, 78]
Unsaturated fatty acids	Neutrophils		[21]
	AgX63.653 murine spleen myeloma cells		[154]
Autologous monocyte co-culture	Human peripheral blood lymphocytes		[24, 81]
Growth as spheroids	GaMG human glioma cell line		[155]
Senescence, extended passaging	Human fibroblasts		[82]
Anticancer drugs and inhibitors			
Antimetabolites			
5-fluorouracil	Transformed HBL-100 breast cells	Chlorpromazine	[70, 87]
Microtubule stabilizers			
Paclitaxel	Human erythroleukemia K562 cells		[73]
Liposome encapsulated	BT-20, MCF-7 breast cancer cells		[76]
Microtubule depolymerizers			
Colcemid	Jurkat T lymphoblasts		[72]
Topisomerase II inhibitors			
Etoposide	HeLa cervical carcinoma cells		[74]
	Murine EL-4 lymphoma cells		[95]
Antitumor antibiotics			
Daunorubicin	Jurkat T lymphoblasts		[40, 72]
Doxorubicin	Jurkat T lymphoblasts		[40, 71, 72]
	Daudi B-lymphoma		[72]
	JY lymphoblastic leukemia		[72]
	HL60 leukemia cells	Bcl-2 transfection	[71, 72, 75]
Glucocorticoids	Jurkat T lymphoblasts		[40, 72]
Dexamethasone			
Fas monoclonal antibodies	Jurkat T lymphoblasts		[48]
	Hut 78, human lymphoblast cell line	Triacsin C	[85]
Differentiating agents			

Mobile Lipid Effector	Cell/Tissue Type	Mobile Lipid Inhibitor	Reference
Phenylacetate	DU145 prostate cells		[46]
Phenylbutyrate		PPAR-γ antagonists	[45, 46, 77]
		AACOCF3	[88]
Cationic lipophilic phosphonium salts	DU4475 breast cancer cells		[20, 70]
	Transformed HBL-100 breast cells	Chlorpromazine	[2, 47, 69, 70]
Cyclosporin A	Transformed HBL-100 breast cells	Chlorpromazine	[86]
Cell cycle blockers			[1]
Desferrioxamine, ADR 529	2609 Glioma cells		[152]
Lonidamine	HeLa cells		
PC-PLC inhibitors			
D-609	NIH-3T3 mouse embryo fibroblasts	*Ras*-transformation	[83, 84]
Thiazolidinediones			
Troglitazone	3T3 F442A cells		[156]

Mitogens and Cytokines			
Phorbol myristate acetate ± ionomycin	Jurkat T lymphoblasts		[40, 157]
	Murine splenic and thymic T cells		[22, 23, 79, 80]
	Human peripheral blood lymphocytes		[81]
Concanavalin A	Murine splenic T cells		[22, 26, 78]
Anti-CD3 antibodies	Murine splenic and thymic T cells	D-609	[80]
	Human peripheral blood lymphocytes		[80, 81]
Lipopolysaccharide	Murine splenic B cells, Human neutrophils		[21, 26, 158, 159]
Interferon-γ	Mouse peritoneal macrophages		[24, 25]

Other			
Listeria monocytogenes	Mouse peritoneal macrophages		[24, 25]
Ionizing radiation	HL60 leukemia cells		[75]
	MG-63 human osteosarcoma spheroids		[160, 161]
HIV-1 infection	Lymphoblastoid cells	Transient	[162]
Bacterial infection	Human neutrophils		[159]
Caveolin-1 transfection	K562 myelogenous leukemia cells		[163]
	K562 myelogenous leukemia cells	Taxol adriamycin resistance	[164]
	MCF-7 breast cells, LoVo colon adenocarcinoma cells	Multidrug resistance	[165]